

⁸⁹Zr-DFO-AMG102 Immuno-PET to Determine Local HGF Protein Levels in Tumors for Enhanced Patient Selection

Eric W. Price¹, Kathryn E. Carnazza¹, Sean D. Carlin¹, Andrew Cho¹, Kimberly J. Edwards¹, Kuntal K. Sevak¹, Jonathan M. Glaser¹, Elisa de Stanchina², Yelena Y. Janjigian^{*3}, and Jason S. Lewis^{*,1,4}

¹Department of Radiology, Memorial Sloan Kettering Cancer Center, New York, New York, USA

²Antitumor Assessment Core Facility, Molecular Pharmacology Program, Memorial Sloan Kettering Cancer Center, New York, New York, USA

³Gastrointestinal Oncology Service, Memorial Sloan Kettering Cancer Center, New York, New York, USA

⁴Program in Molecular Pharmacology, Memorial Sloan Kettering Cancer Center, New York, New York, USA

Corresponding author

Jason S. Lewis, Department of Radiology, 1275 York Avenue, Memorial Sloan Kettering Cancer Center, NY, 10065, USA, Email: lewisj2@mskcc.org Phone: +1.646.888.3038. Fax: +1.646.888.3059

First author

Eric W. Price, postdoctoral fellow, Department of Radiology, 1275 York Avenue, Memorial Sloan Kettering Cancer Center, NY, 10065, USA, Email: eric.price@usask.ca, Phone: +1.306.966.4788. Fax: +1.306.966.4730

Financial support

Eric W. Price was supported by the Natural Sciences and Engineering Research Council (NSERC) (PDF, 2014-2016). The MSKCC Small-Animal Imaging Core Facility, supported in part by NIH Small-Animal Imaging Research Program (SAIRP) Grant No R24 CA83084 and NIH Center Grant No P30 CA08748, are gratefully acknowledged. The Radiochemistry and Molecular Imaging Probe core is also supported in part by NIH center grant N0P30CA08748.

The Antitumor Assessment Core thanks Core Grant (P30 CA008748), and PDX support from U54 Grant (U54 OD020355).

Key words

AMG102; Rilotumumab; hepatocyte growth factor, HGF; scatter factor, PET; MET; patient-derived xenograft

Disclosures

None.

Abbreviated title

⁸⁹Zr-DFO-AMG102 – PET tracer for HGF

Word Count

6498

ABSTRACT

Objectives

The hepatocyte growth factor (HGF) binding antibody rilotumumab (AMG102) was modified for use as an ^{89}Zr -based immuno-PET (positron emission tomography) imaging agent to non-invasively determine the local levels of HGF protein in tumors. As recent clinical trials of HGF targeting therapies have been largely unsuccessful in several different cancers (e.g., gastric, brain, lung), we have synthesized and validated ^{89}Zr -DFO-AMG102 as a companion diagnostic for improved identification and selection of patients having high local levels of HGF in tumors. To date, patient selection has not been performed using the *local levels of HGF protein in tumors*.

Methods

The chelator *p*-SCN-Bn-DFO was conjugated to AMG102, radiolabeling with ^{89}Zr was performed in high radiochemical yields and purity (>99%), and binding affinity of the modified antibody was confirmed using an enzyme-linked immunosorbent assay (ELISA) type binding assay. PET imaging, biodistribution, autoradiography and immunohistochemistry, and *ex vivo* HGF-ELISA experiments were performed in murine xenografts of U87MG (HGF positive (+), MET positive (+)), MKN45 (HGF negative (-), MET +), and 4 patient-derived xenografts (PDX, MET+, HGF unknown).

Results

Tumor uptake of ^{89}Zr -DFO-AMG102 at 120 h p.i. in U87MG xenografts (HGF+) was high (36.8 ± 7.8 % injected dose per gram (ID/g)), while uptake in MKN45 xenografts (HGF-) was 5.0 ± 1.3 %ID/g, and a control of non-specific human IgG ^{89}Zr -DFO-IgG in U87MG tumors was 11.5 ± 3.3 %ID/g, demonstrating selective uptake in HGF+ tumors. Similar experiments performed in 4 different gastric cancer PDX models showed low uptake of ^{89}Zr -DFO-AMG102 (~4-7 %ID/g), which corresponded with low HGF levels in these tumors (*ex vivo* ELISA). Autoradiography, immunohistochemical staining, and HGF-ELISA assays confirmed that elevated levels of HGF

protein were only present in U87MG tumors, and that ^{89}Zr -DFO-AMG102 uptake was closely correlated with HGF protein levels in tumors.

Conclusions

The new immuno-PET imaging agent ^{89}Zr -DFO-AMG102 was successfully synthesized, radiolabeled, and validated *in vitro* and *in vivo* to selectively accumulate in tumors with high local levels of HGF protein. These results suggest that ^{89}Zr -DFO-AMG102 would be a valuable companion diagnostic tool for the non-invasive selection of patients with elevated local concentrations of HGF in tumors for planning any HGF-targeted therapy, with the potential to improve clinical outcomes.

INTRODUCTION

HGF, also called scatter factor, is a heterodimer protein which is normally synthesized by mesenchymal cells including cancers such as sarcomas and high-grade gliomas (1-7). The sole receptor for the HGF ligand, MET (c-MET, mesenchymal-epithelial transition factor), is a transmembrane tyrosine kinase, which is normally expressed in epithelial cells (1). Activation of MET by HGF binding results in deleterious effects in many cancers, and deregulation of MET activity is commonly responsible for tumorigenic properties and invasiveness (6). The increased invasive growth observed in tumors when MET is activated (e.g. by HGF binding or constitutive activation) is a result of pleiotropic biological responses, including increased cell scattering, migration, invasion, and proliferation (8). Cancers that overexpress the MET receptor can be activated in a paracrine fashion by HGF produced from healthy mesenchymal cells in adjacent tissue, or by HGF made by mesenchymal cells within the bulk tumor or tumor cells, which results in a destructive autocrine loop for MET activation (9). For example, gliomas that function with these autocrine HGF loops contain higher concentrations of HGF and are more tumorigenic (9). Aggressiveness and invasiveness in MET positive tumors can be experimentally enhanced by activation of MET by addition of HGF, and alternatively can be abolished by addition of HGF-specific inhibitors (10-12).

An understanding of the HGF/MET system reveals it as an obvious target for therapeutic pharmacological intervention, and tyrosine kinase inhibitors as well as monoclonal antibodies (mAbs) have been developed to this end (Fig. 1) (13). A difficulty encountered in this field of study is identifying cancer cell lines – and more critically, patients – that possess autocrine HGF/MET loops and therefore *high local HGF concentrations in tumors*. Administration of HGF neutralizing antibodies (including AMG102) to U118 and U87MG glioblastoma xenografts in mice (possessing autocrine HGF/MET loops) has resulted in reduced tumor growth when compared to an IgG control (14,15). Of 11 human gastric cancer cell lines (carcinomas) tested in a prior study, only SNU-484 was found to have HGF/MET autocrine loops (despite several of

the tested cells lines expressing HGF mRNA) (16). In mouse models of gastric cancer, HGF/MET autocrine production was only found in MKN45 tumors, and found to promote metastasis (17). Although this study suggested that MKN45 gastric cancer cells possess HGF/MET autocrine loops, our assays have found no HGF expression in the MKN45 cells in our possession *in vitro* or *in vivo* (*vide infra*) (17). These examples show the difficulty in finding appropriate cancer models for this system, but also demonstrate the ability of HGF targeting therapies to show the highest levels of efficacy in tumors that possess HGF/MET autocrine activation loops and *high local levels of HGF*. This suggests that these subpopulations of tumors would be ideal candidates for HGF/MET targeted therapies, and patients possessing high local levels of HGF in tumors would be ideal candidates for HGF-targeted treatments.

A large number of cancers have been reported to express HGF and/or MET clinically, and only a small percentage of each cancer type have been reported in patients to express HGF/MET autocrine loops (e.g. lung adenocarcinoma (18), muscle rhabdomyosarcoma (19), breast carcinoma (20), bone osteosarcoma (21), brain glioma (9,22)). A majority of human primary glioma and brain cancer cell lines have been found to produce their own HGF (9,23). The confounding factor in all of these studies is the lack of correlation between *serum* HGF levels and *local* HGF protein levels in tumor tissue. This suggests that there is a pressing need for a non-invasive method for directly measuring local HGF protein levels in tumors prior to administering HGF or MET targeted therapeutic drugs.

The Amgen Inc. antibody AMG102 is a fully human mAb (IgG₂) that binds to and neutralizes HGF, thus preventing its binding to MET and therefore providing therapeutic effects. AMG102 has been tested in clinical trials for a number of different cancers, all with limited success to date. Despite a phase II trial of AMG102 in gastric cancer showing improved overall survival and progression-free survival, a recent phase III clinical trial of AMG102 in gastric cancer was terminated early (24). Because subjects have been evaluated by different methods in various studies — such as serum levels of HGF protein, local levels of MET protein in tumors

(over-expression), and gene amplification (not always accompanied by transcriptional up-regulation and overexpression of protein products) — finding appropriate autocrine HGF/MET cancer types and corresponding models is challenging (25). To our knowledge, patient selection for clinical trials of HGF-targeted drugs has not been attempted by measuring HGF levels directly in tumors, and although increased circulating HGF may be a prognostic factor in many cancers, it may be the wrong parameter to evaluate when investigating HGF-targeting therapies (25). No tools currently exist to non-invasively determine the levels of HGF present in the local tumor environment. Biopsies to measure HGF levels are not routinely performed, and due to the large heterogeneity within single tumors and even between different tumors/metastasis in a single patient, biopsy measurements are not accurate and therefore PET imaging would provide a superior whole-body picture of the HGF status of every lesion. To this end, we have developed an ^{89}Zr -based radioimmunoconjugate from the fully human antibody AMG102 to determine the local levels of HGF in tumors by PET imaging. Previous work towards molecular imaging of HGF is limited to an antibody fragment (nanobody), which has been radiolabeled with ^{89}Zr and used to image HGF in U87MG glioblastoma xenografts with some success (26).

MATERIALS AND METHODS

General Procedures

All experiments were performed under a Memorial Sloan Kettering Institutional Animal Care and Use Committee-approved (IACUC) protocol, and the experiments followed institutional guidelines for the proper and humane use of animals in research, and human tissue samples were collected for the Antitumor Assessment Core Facility under an approved IRB protocol. ^{89}Zr was produced at Memorial Sloan Kettering Cancer Center using an EBCO TR19/9 variable-beam energy cyclotron (EbcO Industries Inc., British Columbia, Canada) via the $^{89}\text{Y}(p,n) ^{89}\text{Zr}$ reaction. ^{89}Zr was purified in accordance with previously reported methods to create ^{89}Zr with a specific activity of 5.3 – 13.4 mCi/ μg (195 – 497 MBq/ μg)(27). Detailed information regarding *in*

in vitro experiments and retrospective analysis of clinical data (Fig. 2) is provided in the Supporting Information.

⁸⁹Zr- Radiolabeling of DFO-AMG102 and DFO-IgG

Aliquots of chelate-modified antibody (350 µg) were transferred to 2 mL microcentrifuge tubes and made up to ~0.5 mL with phosphate buffered saline (PBS, pH 7.4, treated with chelex resin at 1.2 g/L Chelex overnight before use, BioRad Laboratories, Hercules, CA). Aliquots of ⁸⁹Zr oxalate were neutralized to ~pH 7.0-7.4 using sodium carbonate (1 M), and subsequently mixed with the DFO-AMG102 and DFO-IgG samples (~2.0 mCi, ~74 MBq) and reacted for 60 minutes at 37 °C. Radiochemical yields obtained were >98% after 1 hour by radio-iTLC (EDTA mobile phase, 50 mM, pH 5) using silica-gel impregnated glass-microfiber paper strips (iTLC-SG, Varian, Lake Forest, CA) (analyzed by AR-2000, Bioscan Inc., Washington, DC). ⁸⁹Zr labeled antibodies were then purified using size-exclusion chromatography (PD10), followed by centrifugal filtration (Amicon® ultra 50k, with saline) to concentrate the final volume for formulation. The radiochemical purity of the final purified radiolabeled antibodies was confirmed to be >99% by radio-iTLC before injection. The ⁸⁹Zr-DFO-AMG102 radioimmunoconjugate was assessed for stability in human blood serum (Sigma) for 7 days at 37 °C (radio-iTLC).

MKN45 and U87MG Xenograft Mouse Models

Eight- to ten-week-old athymic nu/nu female mice (NCRNU-M) were obtained from Charles River Laboratories (Kingston, NY). Animals were housed in ventilated cages, were given food and water *ad libitum*, and were allowed to acclimatize for approximately 1 week prior to treatment. After several days, MKN45 and U87MG tumors were induced on the left shoulder by a subcutaneous injection of 8.0×10^6 cells in a 100 µL cell suspension of a 1:1 mixture of fresh media/BD Matrigel (BD Biosciences, Bedford, Ma). Experiments were performed ~2 weeks following the injection of the cancer cells.

Patient-derived Xenograft Mouse Models

PDX models were established from tumor specimens collected under an approved IRB protocol.

Briefly, tumors were minced, mixed with matrigel, and implanted subcutaneously in 6-8 weeks old female NSG mice (Jackson labs). Once established, tumors were maintained and expanded by serial subcutaneous transplantation. All patient samples had gastric HER2+ tumors. DF and DY were from the same patient at different stages of disease. Tumor samples were evaluated by IHC and graded for HER2 and MET expression, with DC, DF, DY, and EK all being graded 3+ for HER2 expression (high), and 3+, 1-2+, 2+, and 3+ for MET, respectively. HGF levels in these tumors were not evaluated prior to this study.

⁸⁹Zr-DFO-AMG102 PET Imaging

PET imaging was performed using a micro-PET rodent scanner (Focus 120, Concord Microsystems). Mice were administered radiolabeled antibody (~30 µg, ~130-150 µCi, ~4.8-5.6 MBq) in 200 µL sterile saline (0.9% NaCl) via intravenous tail vein injection. Approximately 5 minutes prior to PET image acquisition, mice were anesthetized via inhalation of 2% isoflurane/oxygen gas mixture (Baxter Healthcare, Deerfield, IL) and placed on the scanner bed where anesthesia was maintained. PET images were acquired at 24, 48, 72, and 120 h, with PET data being recorded via static scans with a minimum of 15 million coincident events (~20-30 minutes). An energy window of 350-700 keV and a coincidence timing window of 6 ns was used. Data was sorted into 2D histograms by Fourier rebinning, and transverse images were reconstructed by filtered back-projection (FBP) into a 128 x 128 x 63 (0.72 x 0.72 x 1.3 mm³) matrix. The image data was normalized to correct for non-uniformity of response of the PET, dead-time count losses, positron branching ratio, and physical decay to the time of injection, but no attenuation, scatter, or partial-volume averaging correction was applied. The counting rates in the reconstructed images were converted to activity concentrations (percentage injected dose [%ID] per gram of tissue) by use of a system calibration factor derived from the imaging of a mouse-sized water-equivalent phantom containing ⁸⁹Zr. Images were analyzed using ASIPro VM software (Concorde Microsystems).

⁸⁹Zr-DFO-AMG102 and ⁸⁹Zr-DFO-IgG Biodistribution Studies

Mice bearing subcutaneous xenografts as described above were intravenously injected through the tail vein with either ^{89}Zr -DFO-AMG102 or ^{89}Zr -DFO-IgG ($\sim 20\text{-}30\ \mu\text{Ci}$, $0.74\text{-}1.1\ \text{MBq}$, $\sim 5\ \mu\text{g}$, in $200\text{-}250\ \mu\text{L}$ of sterile saline; tumor volume $\sim 100\text{-}150\ \text{mm}^3$). Mice were euthanized by CO_2 (g) asphyxiation at time points of 24, 48, 72, and 120 hours ($n = 5$ per time point). Organs collected after sacrifice included blood, tumor, heart, lungs, liver, spleen, pancreas, kidneys, large intestine, small intestine, muscle, bone (femur), and skin (ear). All organs were rinsed in water after removal and air-dried for 5 minutes. The organs from ^{89}Zr biodistribution experiments were placed in pre-weighed test tubes, weighed again to obtain tissue weights, and the amount of radioactivity present was determined using a Perkin-Elmer (Waltham, MA) Automated Wizard Gamma Counter. The counts were background- and decay-corrected from the time of injection and then converted to the percentage of injected dose (%ID) per gram of organ tissue (%ID/g). The radioactivity counts measured in each organ were converted to activity (μCi) using a calibration curve created from known standards of ^{89}Zr (serial dilution from $\sim 3\ \mu\text{Ci}\ ^{89}\text{Zr}$). The gastric cancer PDX mice (DF, DY, DC, EK) imaged with ^{89}Zr -DFO-AMG102 were euthanized for biodistribution experiments immediately following their final imaging point (120 h).

Autoradiography and Histology

Following PET imaging and excision of tumors, a subset of tumors were embedded in optimal-cutting-temperature mounting medium (OCT, Sakura Finetek) and frozen on dry ice. Series of $10\ \mu\text{m}$ frozen sections were then cut. To determine radiotracer distribution, digital autoradiography was performed by placing tissue sections in a film cassette against a phosphor imaging plate (Fujifilm BAS-MS2325; Fuji Photo Film) for an appropriate exposure period at $-20\ ^\circ\text{C}$. Phosphor imaging plates were read at a pixel resolution of $25\ \mu\text{m}$ with a Typhoon 7000 IP plate reader (GE Healthcare). After autoradiographic exposure, the same frozen sections were then used for immunohistochemical (IHC) staining and microscopy. Immunohistochemical staining of HGF and Perlecan was carried out using antibodies LS-B4957 (1:50 dilution,

Lifespan Biosciences) and A7L6 (5 µg/ml, ThermoFisher) respectively, and secondary detection with species-appropriate secondary antibodies conjugated to Alexafluor-568 and Alexafluor-488 respectively. Sequential sections were stained with H&E.

Whole mount images were acquired at ×100 magnification using a BX60 microscope (Olympus America, Inc.) equipped with a motorized stage (Prior Scientific Instruments Ltd.) and DP80 camera (Olympus). Whole-tumor montage images were obtained by acquiring multiple fields at ×40 magnification, followed by alignment using MicroSuite Biologic Suite (version 2.7; Olympus). IHC and autoradiographic images were registered using Adobe Photoshop (CS6) as previously described (28).

RESULTS AND DISCUSSION

Retrospective Analysis of Clinical Patient Data

An evaluation of publicly available patient data on HGF mRNA expression and phosphoMET protein levels was performed to highlight relevant cancers for HGF-targeted drugs, as clinical trials of HGF-targeted drugs have been relatively unsuccessful to date (Fig. 2). Microchip-mRNA data suggests that lung adenocarcinoma (sample size 32), glioblastoma multiforme (sample size 473), and kidney renal clear cell carcinoma (sample size 72) have statistically significantly higher levels of HGF mRNA than the other displayed cancer types, suggesting these cancers as clinically relevant subjects for future investigations of HGF-targeting drugs (Fig. 2A). More relevant for this study, protein levels of phosphoMET (activated MET, typically via HGF binding) in gastric cancer shows a significant trend between phosphoMET quantile levels and survival. When activated by HGF binding, the MET receptor (tyrosine kinase) becomes phosphorylated as phosphoMET, suggesting a correlation between high levels of phosphoMET and HGF. Decreased survival times are observed between patients with higher phosphoMET protein levels (Q1 median survival 609 days) compared with lower levels (Q4 median survival 881 days) (Fig. 2B). This analysis of clinical data highlights the critical role of HGF and activated

phosphoMET in tumor aggression and survival times, and supports the hypothesis that local HGF protein levels should be evaluated in patient tumors prior to administering HGF-targeted therapies.

Bioconjugation, Radiolabeling, and *In Vitro* Characterization

To begin, AMG102 was incubated under slightly basic conditions (pH. 9.0) with 5 equivalents of *p*-SCN-Bn-DFO and purified via size exclusion chromatography (PD10) and spin filtration (Amicon Ultra 50 kDa). After purification, aliquots of AMG102 immunoconjugates were frozen and sent for analysis by matrix-assisted laser desorption/ionization time-of-flight (MALDI-TOF) mass spectrometry analysis. Mass spectrometry results indicated that these modifications yielded 1.0 ± 0.1 chelates per antibody (Supplemental Figs. 1-6; Supplemental Table 1). Determination of immunoreactivity (e.g. immunoreactive fraction) could not be performed by a standard immunoreactivity cell-binding assay(29), as the target antigen HGF is a circulating growth factor and not a cell surface-bound receptor. An ELISA-based binding assay was therefore performed to compare binding affinity values of AMG102, DFO-AMG102, and a non-specific human IgG, which confirmed little change in binding affinity for DFO-AMG102 (0.64 vs 0.83 nM K_d , literature 0.22 nM (3)) (Fig. 3B). DFO-AMG102 was then radiolabeled with ^{89}Zr in PBS (pH 7.4, treated with Chelex resin) for 60 min at 37 °C. Radiochemical yields (RCY) were evaluated using radio-iTLC, and a mobile phase of EDTA (pH 5, 50 mM) was used to resolve “free” ^{89}Zr from antibody-bound radiometal, which confirmed >98% crude RCY and >99% radiochemical purity (RCP) after PD10 purification (Fig. 3A). Before utilizing the new radioimmunoconjugate ^{89}Zr -DFO-AMG102, appropriate cancer models were selected. Available gastric cancer cell lines were grown in culture, and the spent media (5 days incubation time) was harvested and analyzed by ELISA for HGF content. It was determined that the only cell line producing detectable quantities of HGF was U87MG glioblastoma, which has been previously studied in the literature with HGF targeting antibodies (Fig. 3D). Because the antibody AMG102 does not recognize or bind murine HGF, a suitable cell line was required for this initial study that

possessed an autocrine HGF/MET loop and therefore would contain high local levels of HGF in tumor models (6,8), and so U87MG cells were selected. MET expression in U87MG (HGF+) and MKN45 (HGF-) cells was confirmed by western blot analysis (Fig. 3C).

⁸⁹Zr-DFO-AMG102 PET Imaging Studies in U87MG and MKN45 Murine Subcutaneous Xenografts

Female nude athymic mice were inoculated with subcutaneous xenografts (8×10^6 cells, left shoulder) of U87MG (HGF+, MET+, n=4) or MKN45 (HGF-, MET+, n=4, controls) tumors, and ⁸⁹Zr-DFO-AMG102 was administered via intravenous tail vein injection for serial PET imaging studies (~30 µg, ~130-150 µCi, ~4.8-5.6 MBq, 200 µL sterile saline). PET images were acquired at 24, 48, 72, and 120 h post injection, showing a steady increase in U87MG tumor uptake (~40 %ID/g at 120 h p.i.) with a concomitant decrease in blood pool/background activity during the 120 h imaging study (Fig. 4). Control images obtained in mice bearing MKN45 xenografts revealed high blood pool and background activity at all time points, with tumor uptake remaining low at 5-10 %ID/g throughout the duration of the study (Fig. 4). This experiment demonstrates that uptake of ⁸⁹Zr-DFO-AMG102 is very low (background uptake, from enhanced permeability and retention (EPR) effect) in tumors that do not contain high local concentrations of HGF (MKN45), whereas uptake is high in tumors which contain high local levels of HGF (U87MG).

Biodistribution Studies of ⁸⁹Zr-DFO-AMG102

Radiolabeled and purified ⁸⁹Zr-DFO-AMG102 was injected via tail vein into mice bearing subcutaneous U87MG (autocrine, HGF+, MET+, n=5) or MKN45 (HGF-, MET+, n=10, control) xenografts on the left shoulder (~20-30 µCi, 0.74-1.1 MBq, ~5 µg, in 200-250 µL of sterile saline; tumor volume ~100-150 mm³). After time points of 24, 48, 72, and 120 h (n = 5 per time point), the mice were euthanized via CO₂ (g) asphyxiation followed by cervical dislocation, after which 14 organs including the tumors were removed, weighed, and assayed for radioactivity using an automated gamma counter. Control biodistributions were performed in U87MG tumor-bearing mice with both ⁸⁹Zr-DFO-IgG (non-specific isotype human IgG), and a blocking group

that was co-injected with “cold” AMG102 (100 fold, 500 μ g). These controls were performed to confirm selective uptake of ^{89}Zr -DFO-AMG102 in HGF positive tumors beyond uptake from the EPR effect. Biodistribution data demonstrated substantial uptake of ^{89}Zr -DFO-AMG102 in HGF positive tumors (U87MG), reaching 36.8 ± 7.8 %ID/g at 120 h p.i. (Supplemental Tables 2-5). This result compared favorably with two controls that showed low tumor uptake values of 5.0 ± 1.3 %ID/g and 11.5 ± 3.3 %ID/g for HGF negative tumors (MKN45) and ^{89}Zr -DFO-IgG in U87MG tumors, respectively. Organ ratios were calculated from ^{89}Zr -DFO-AMG102 biodistribution data and revealed tumor-to-blood (T/B), tumor-to-heart (T/H), and tumor-to-liver (T/L) ratios to be excellent in U87MG tumors when compared to MKN45 controls (T/B = 2.4 ± 0.6 vs 0.4 ± 0.1 , T/H = 7.5 ± 1.6 vs 1.7 ± 0.5 , T/L = 6.6 ± 1.5 vs 1.0 ± 0.4 , respectively, Supplemental Table 5). Blocking appears unsuccessful when looking at tissue-weight normalized uptake values (%ID/g, Fig. 5A), Supplemental Fig. 7A shows this same data as non-normalized uptake values (%ID), which suggests at least partial blocking of tumor uptake. This could be a result of the dramatic therapeutic effect observed from the blocking dose of AMG102 (500 μ g), which resulted in a substantial decrease in tumor size (0.06 ± 0.03 g blocking vs 0.21 ± 0.05 g non-blocking, n = 5, Supplemental Fig. 7B). Although the tissue-weight normalization (%ID/g) should account for this tumor size difference, such a dramatic difference in tumor size doesn't appear to be appropriately corrected for, possibly due to high levels antigen (HGF) and the small injected dose of antibody (~ 5 μ g) not saturating target binding (HGF) in either scenario. Further to this point, the biodistribution blocking data shown in Supplemental Fig. 7A as %ID reveals equivalent uptake in all organs except the tumor (statistically significantly lower uptake in blocked tumor). Not all targets can effectively be blocked with reasonable doses, and due to the high levels of HGF produced by U87MG tumors, the blocking dose of 500 μ g may not have been sufficient. Problematically, this dose was sufficient for a dramatic therapeutic effect (Supplemental Fig. 7B), suggesting that blocking studies are not effective controls for this

specific imaging agent. It has been previously shown in mice bearing xenografts of U87MG cells that AMG102 has a substantial therapeutic effect when compared to control groups (15), and these results were confirmed during this study (Supplemental Fig. 7B).

These non-standard blocking results are not entirely convincing, but are also not of serious concern because a second control experiment was performed and successfully demonstrated selective uptake of ^{89}Zr -DFO-AMG102 in tumors with high HGF levels (U87MG, 36.8 ± 7.8 %ID/g, 120h p.i.) and low uptake in HGF negative tumors (MKN45, 5.0 ± 1.3 %ID/g, 120h p.i.) by both PET imaging and biodistribution studies (HGF levels quantitatively confirmed by ELISA assay, Figs. 4 and 5B). A third control experiment was also successful and demonstrated lower uptake of a non-specific isotype control antibody ^{89}Zr -DFO-IgG in HGF positive U87MG tumor xenografts (11.5 ± 3.3 %ID/g, 120h p.i.) compared to ^{89}Zr -DFO-AMG102 (36.8 ± 7.8 %ID/g, 120h p.i.) via biodistribution of tumor-bearing mice (Fig. 5A).

^{89}Zr -DFO-AMG102 PET Imaging in Patient-derived Xenografts

To evaluate the ability of ^{89}Zr -DFO-AMG102 to non-invasively determine local HGF protein levels in tumors, four different PDXs were obtained that all had confirmed MET expression by IHC, but had unknown levels of HGF. Only a small number of PDX bearing mice were available, and some were bilateral xenografts that contained the same PDX tumor type on both flanks. The radioimmunoconjugate ^{89}Zr -DFO-AMG102 was prepared and injected as described above, and serial PET imaging was performed at 24, 48, 72, and 120 h, with necropsy, tissue harvesting, and biodistribution analysis performed following 120 h PET imaging. The PET images in Fig. 6 are all 120 h p.i. and are compared to U87MG (HGF+ control) and MKN45 (HGF- control) xenografts, with PDX tumor uptake ranging between 5-10 %ID/g. These PDX PET imaging results suggest the limited uptake of ^{89}Zr -DFO-AMG102 was largely a result of non-specific EPR uptake (as with control experiments), and the range in uptake between 5-10 %ID/g is likely attributed to variations in vasculature and blood flow between these different PDX tumors (full time-course images Supplemental Figs 8 and 9). Because successful control

experiments with ^{89}Zr -DFO-AMG102 have demonstrated it to be selective for HGF+ tumors, these results provide a non-invasive measure of the levels of HGF protein in these PDX tumors. These results suggest that these specific PDX contain low-levels of HGF protein and therefore would not be suitable candidates for administration of a therapeutic regimen of AMG102 or any other HGF-targeting drug, as they would not be likely to respond.

^{89}Zr -DFO-AMG102 Biodistribution, Autoradiography, and Immunohistochemistry in Patient-derived Xenografts

Biodistribution experiments were performed on the PDX bearing mice shown in Fig. 6, following 120 h PET imaging. The uptake of ^{89}Zr -DFO-AMG102 in PDX tumors was confirmed to be low (~4-7 %ID/g), which corroborates the PET imaging data displayed in Fig. 6 that suggested low uptake of ~5-10%ID/g (non-specific EPR uptake) (Fig. 5B, data in Supplemental Table 6). To validate these results using additional quantitative methods, tumor and blood serum samples were obtained from mice bearing PDX and U87MG/MKN45 tumors, and were analyzed using an ELISA kit for HGF. The ELISA results confirm that the only tumors that contained high levels of HGF were U87MG (3.31 ng/mg of protein), with MKN45 and PDX tumors containing HGF levels of only 0.02-0.26 ng/mg of protein, which aligns well with reported normal levels of HGF in human tissue of 0.22 ± 0.32 ng/mg of protein (Fig. 5C) (17,30). The HGF protein concentrations determined by ELISA aligned well with the observed tumor uptake values (%ID/g) of ^{89}Zr -DFO-AMG102 in tumors by PET imaging and biodistributions (Figs. 5C and 6). These results in U87MG xenografts reveal that despite having high intratumoral HGF protein levels, no HGF could be detected in blood serum (Fig. 5C). This study provides further credence to the idea that *local* HGF protein levels in tumors must be assessed, as serum levels may not accurately predict intratumoral levels.

During tissue harvesting and biodistribution analysis, tumor sections were taken and autoradiography and IHC was performed on the ^{89}Zr -DFO-AMG102 containing samples (Fig. 7). Autoradiography and IHC demonstrated uptake of ^{89}Zr -DFO-AMG102 largely in the stroma and

areas of vasculature (basement membrane/extracellular matrix) of the MKN45 (HGF-) tumors, which would be consistent with non-specific EPR uptake (Fig. 7). Of interest is the fact that HGF is a low affinity binder to the glycoprotein heparin sulfate, which retains HGF in the stroma and limits diffusion out of the tumors (31). These tumor sections were additionally stained for perlecan (green, heparin sulfate glycoprotein in stroma) and human HGF (red), to see if co-localization could be observed. No significant co-localization of ^{89}Zr -DFO-AMG102, HGF, and perlecan could be observed from this immunofluorescent staining (Fig. 7). High levels of HGF in U87MG tumor sections relative to MKN45 tumors was confirmed, which also mimics autoradiography results showing higher uptake of ^{89}Zr -DFO-AMG102 selectively in U87MG tumors. Similar autoradiography and immunofluorescence staining was performed on PDX tumor sections, which confirmed low uptake of ^{89}Zr -DFO-AMG102 and low levels of HGF (Supplemental Figs. 10-12).

CONCLUSIONS

The HGF binding antibody AMG102 was successfully modified for use as an ^{89}Zr -based immuno-PET imaging agent to non-invasively determine local HGF protein levels in tumors. Uptake of ^{89}Zr -DFO-AMG102 at 120 h p.i. in U87MG (HGF+) xenografts (36.8 ± 7.8 %ID/g) was statistically significantly higher than in control tumors (MKN45, HGF-, 5.0 ± 1.3 %ID/g), ^{89}Zr -DFO-IgG non-specific isotype control in U87MG (11.5 ± 3.3 %ID/g). Similar experiments performed in 4 different gastric cancer PDX models showed low uptake of ^{89}Zr -DFO-AMG102 ($\sim 4\text{-}7$ %ID/g), which corresponded with low HGF levels in these tumors as determined by ELISA assay of tumor homogenates and serum samples. Taken together, these results craft a compelling story that the new immuno-PET imaging agent ^{89}Zr -DFO-AMG102 would be a valuable companion diagnostic tool for selection of patients that possess high local HGF protein levels in tumors, and would therefore be more likely to respond to any HGF-targeted therapy.

ACKNOWLEDGEMENTS

The authors acknowledge Dr. Kristen Cunanan (MSKCC, Epidemiology & Biostatistics) for assistance in reporting the statistical analysis of clinical patient data, and Dr. Freddy Escorcia (MSKCC, Radiation Oncology) for thoughtful editing.

REFERENCES

1. Bottaro D, Rubin J, Faletto D, et al. Identification of the hepatocyte growth factor receptor as the c-met proto-oncogene product. *Science*. 1991;251:802-804.
2. Cecchi F, Rabe DC, Bottaro DP. Targeting the HGF/Met signaling pathway in cancer therapy. *Expert Opin Ther Targets*. 2012;16:553-572.
3. Cecchi F, Rabe DC, Bottaro DP. The Hepatocyte Growth Factor Receptor: Structure, Function and Pharmacological Targeting in Cancer. *Curr Signal Transduction Ther*. 2011;6:146-151.
4. Cecchi F, Rabe DC, Bottaro DP. Targeting the HGF/Met signalling pathway in cancer. *Eur J Cancer*. 2010;46:1260-1270.
5. Jiang WG, Martin TA, Parr C, Davies G, Matsumoto K, Nakamura T. Hepatocyte growth factor, its receptor, and their potential value in cancer therapies. *Crit Rev Oncol Hematol*. 2005;53:35-69.
6. Corso S, Comoglio PM, Giordano S. Cancer therapy: can the challenge be MET? *Trends Mol Med*. 2005;11:284-292.
7. Comoglio PM, Boccaccio C. Scatter factors and invasive growth. *Semin Cancer Biol*. 2001;11:153-165.
8. Giordano S. Rilotumumab, a mAb against human hepatocyte growth factor for the treatment of cancer. *Curr Opin Mol Ther*. 2009;11:448-455.
9. Koochekpour S, Jeffers M, Rulong S, et al. Met and hepatocyte growth factor/scatter factor expression in human gliomas. *Cancer Res*. 1997;57:5391-5398.
10. Michieli P, Basilico C, Pennacchietti S, et al. Mutant Met-mediated transformation is ligand-dependent and can be inhibited by HGF antagonists. *Oncogene*. 1999;18:5221-5231.
11. Rong S, Segal S, Anver M, Resau JH, Vande Woude GF. Invasiveness and metastasis of NIH 3T3 cells induced by Met-hepatocyte growth factor/scatter factor autocrine stimulation. *Proc Natl Acad Sci U S A*. 1994;91:4731-4735.
12. Abounader R, Lal B, Luddy C, et al. In vivo targeting of SF/HGF and c-met expression via U1snRNA/ribozymes inhibits glioma growth and angiogenesis and promotes apoptosis. *The FASEB Journal*. 2001;16:108-110.
13. Scagliotti GV, Novello S, von Pawel J. The emerging role of MET/HGF inhibitors in oncology. *Cancer Treat Rev*. 2013;39:793-801.
14. Cao B, Su Y, Oskarsson M, et al. Neutralizing monoclonal antibodies to hepatocyte growth factor/scatter factor (HGF/SF) display antitumor activity in animal models. *Proceedings of the National Academy of Sciences*. 2001;98:7443-7448.

15. Rex K, Lewis XZ, Gobalakrishnan S, et al. Evaluation of the antitumor effects of rilotumumab by PET imaging in a U-87 MG mouse xenograft model. *Nucl Med Biol.* 2013;40:458-463.
16. Park M, Park H, Kim W-H, Cho H, Lee J-H. Presence of autocrine hepatocyte growth factor-Met signaling and its role in proliferation and migration of SNU-484 gastric cancer cell line. *Exp Mol Med.* 2005;37:213-219.
17. Toiyama Y, Yasuda H, Saigusa S, et al. Co-expression of hepatocyte growth factor and c-Met predicts peritoneal dissemination established by autocrine hepatocyte growth factor/c-Met signaling in gastric cancer. *Int J Cancer.* 2012;130:2912-2921.
18. Siegfried JM, Weissfeld LA, Singh-Kaw P, Weyant RJ, Testa JR, Landreneau RJ. Association of Immunoreactive Hepatocyte Growth Factor with Poor Survival in Resectable Non-Small Cell Lung Cancer. *Cancer Res.* 1997;57:433-439.
19. Ferracini R, Olivero M, Di Renzo MF, et al. Retrogenic expression of the MET proto-oncogene correlates with the invasive phenotype of human rhabdomyosarcomas. *Oncogene.* 1996;12:1697-1705.
20. Tuck AB, Park M, Sterns EE, Boag A, Elliott BE. Coexpression of hepatocyte growth factor and receptor (Met) in human breast carcinoma. *The American Journal of Pathology.* 1996;148:225-232.
21. Ferracini R, Di Renzo MF, Scotlandi K, et al. The Met/HGF receptor is over-expressed in human osteosarcomas and is activated by either a paracrine or an autocrine circuit. *Oncogene.* 1995;10:739-749.
22. Birchmeier C, Birchmeier W, Gherardi E, Vande Woude GF. Met, metastasis, motility and more. *Nat Rev Mol Cell Biol.* 2003;4:915-925.
23. Rosen EM, Laterra J, Joseph A, et al. Scatter factor expression and regulation in human glial tumors. *Int J Cancer.* 1996;67:248-255.
24. Cunningham D, Tebbutt NC, Davidenko I, et al. Phase III, randomized, double-blind, multicenter, placebo (P)-controlled trial of rilotumumab (R) plus epirubicin, cisplatin and capecitabine (ECX) as first-line therapy in patients (pts) with advanced MET-positive (pos) gastric or gastroesophageal junction (G/GEJ) cancer: RILOMET-1 study. *Journal Clin Oncol.* 2015:abstract 4000.
25. Zhang Y, Jain R, Zhu M. Recent Progress and Advances in HGF/MET-Targeted Therapeutic Agents for Cancer Treatment. *Biomedicines.* 2015;3:149-181.
26. Vosjan MJWD, Vercammen J, Kolkman JA, Stigter-van Walsum M, Revets H, van Dongen GAMS. Nanobodies Targeting the Hepatocyte Growth Factor: Potential New Drugs for Molecular Cancer Therapy. *Mol Cancer Ther.* 2012;11:1017-1025.
27. Holland JP, Sheh Y, Lewis JS. Standardized methods for the production of high specific-activity zirconium-89. *Nucl Med Biol.* 2009;36:729-739.

- 28.** Carlin S, Zhang H, Reese M, Ramos NN, Chen Q, Ricketts S-A. A Comparison of the Imaging Characteristics and Microregional Distribution of 4 Hypoxia PET Tracers. *J Nucl Med.* 2014;55:515-521.
- 29.** Lindmo T, Boven E, Cuttitta F, Fedorko J, Bunn Jr PA. Determination of the immunoreactive function of radiolabeled monoclonal antibodies by linear extrapolation to binding at infinite antigen excess. *J Immunol Methods.* 1984;72:77-89.
- 30.** Toiyama Y, Miki C, Inoue Y, Okugawa Y, Tanaka K, Kusunoki M. Serum hepatocyte growth factor as a prognostic marker for stage II or III colorectal cancer patients. *Int J Cancer.* 2009;125:1657-1662.
- 31.** To CT, Tsao MS. The roles of hepatocyte growth factor/scatter factor and met receptor in human cancers (Review). *Oncol Rep.* 1998;5:1013-1024.

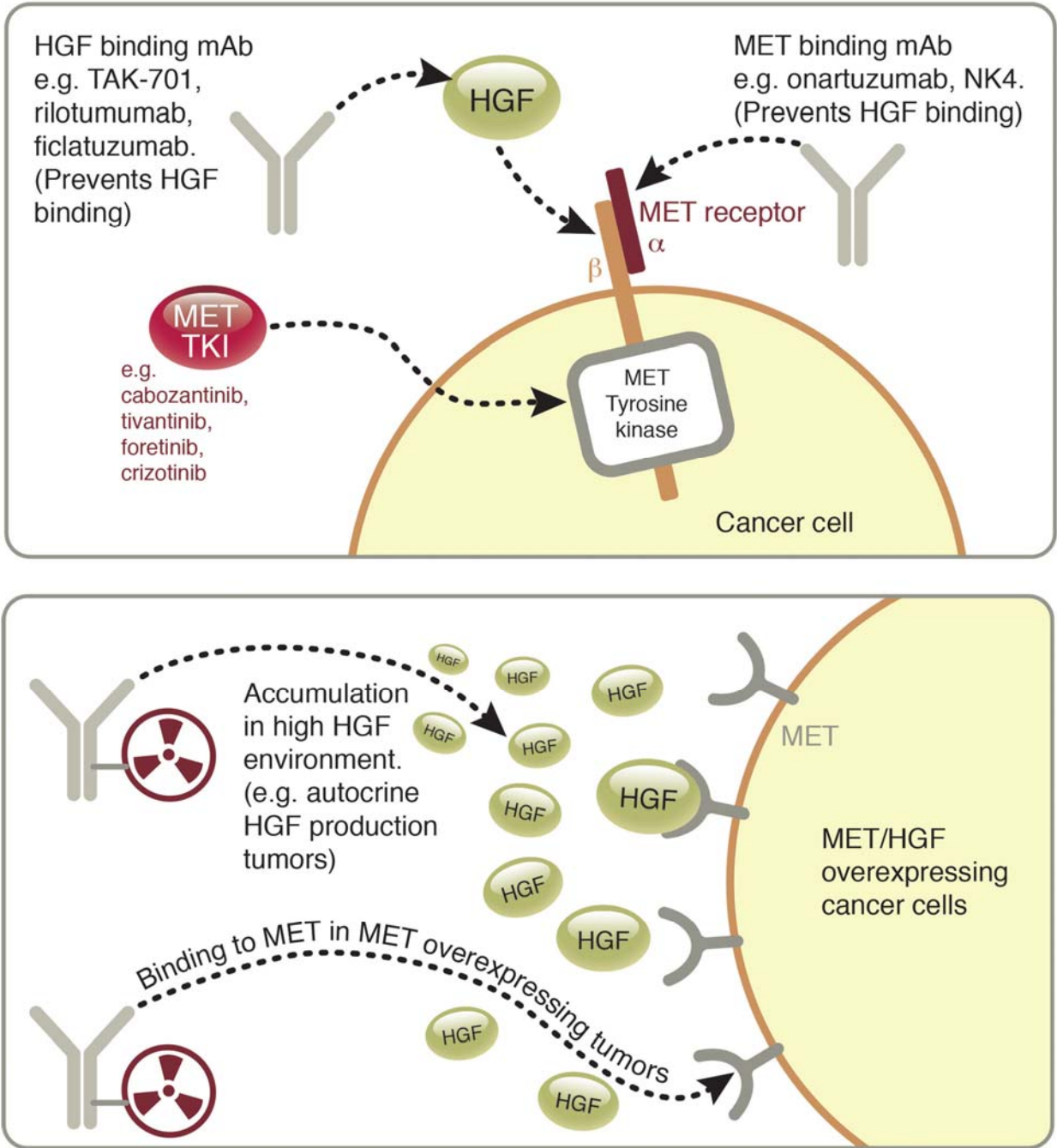


Fig. 1. A graphic of the MET/HGF system illustrating the therapeutic approaches currently used to target it (top panel), including HGF binding/neutralizing antibodies, MET binding antagonists, and MET tyrosine kinase inhibitors, and a depiction of antibodies tagged with a radioactive metal (⁸⁹Zr) for use in immuno-PET of HGF/MET positive cancers (bottom).

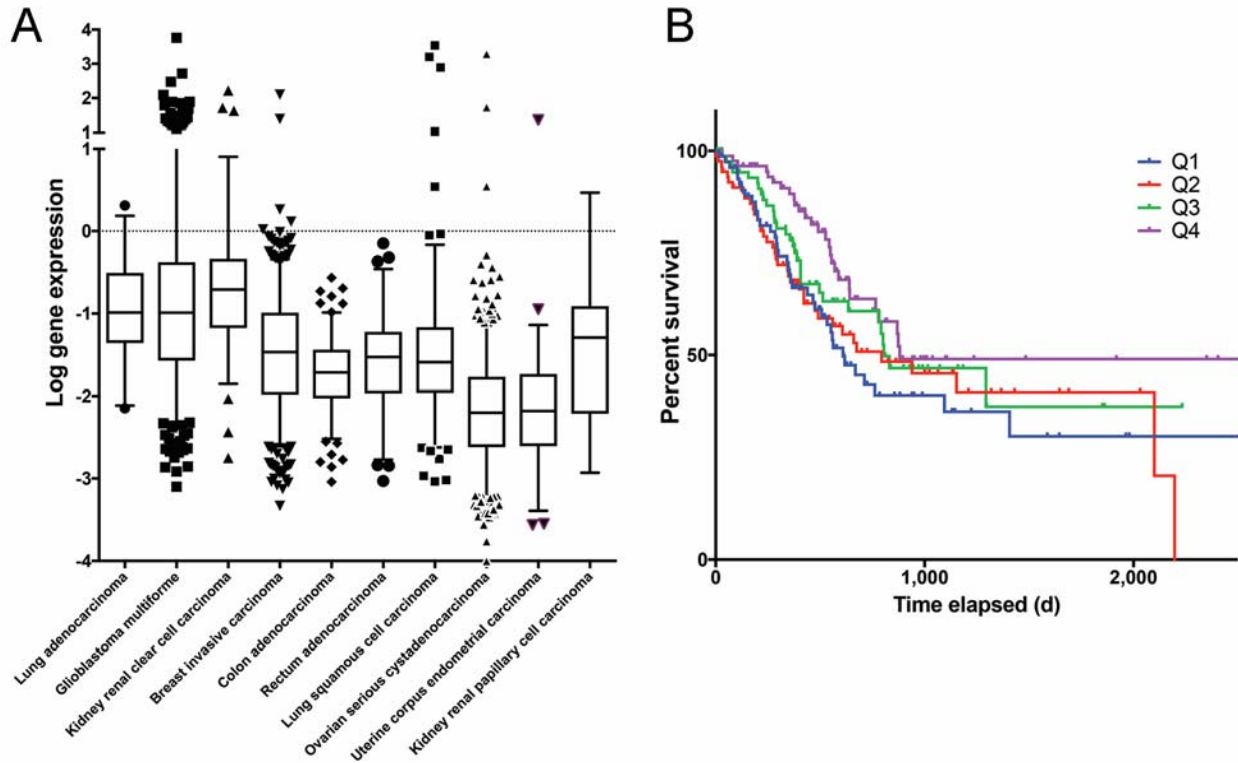


Fig. 2. Evaluation of clinical patient data showing (A) HGF mRNA levels in patients from micro-mRNA chip array data, showing a statistically significantly higher level of HGF mRNA expression (unadjusted p-values <0.00001-0.00005, significant by 1-sided and 2-sided t-tests, no correction for multiple comparisons) in lung adenocarcinoma (sample size 32), glioblastoma multiforme (sample size 473), and kidney renal clear cell carcinoma (sample size 72) when compared to other cancer types displayed (no data for gastric cancer was available), and (B) survival curve for patients relating to protein levels of phosphoMET (activated MET receptor, usually by HGF binding) in gastric cancer patients, showing significance at 5% alpha level by log-rank test for trend between the four quantile groups in survival times (top Q1 median survival 609 days, bottom Q4 median survival 881 days, 357 subjects) of phosphoMET levels. The results shown and discussed here are in whole or part based upon data generated by the TCGA Research Network: <http://cancergenome.nih.gov/>.

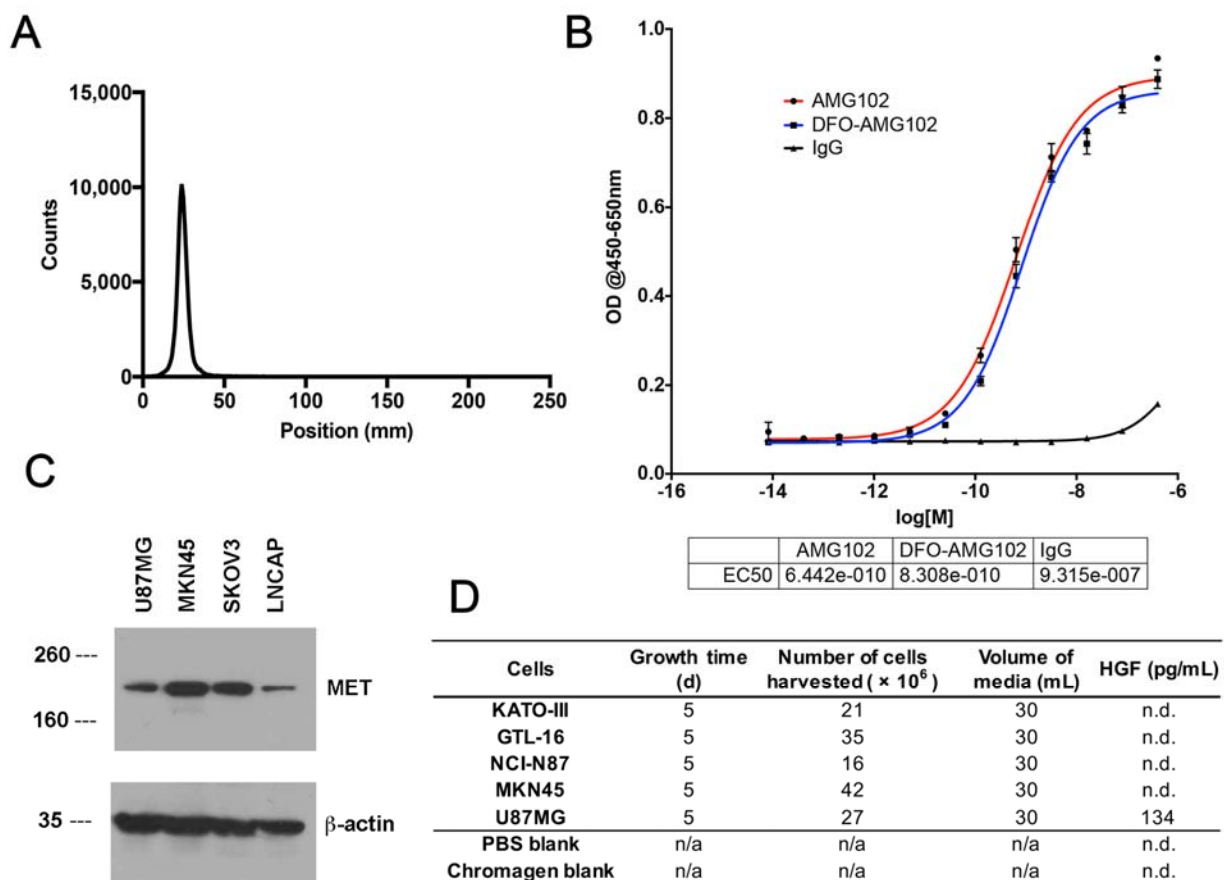


Fig. 3. Results for radiolabeling, binding affinity, and cancer cell line selection; (A) ^{89}Zr -DFO-AMG102 radiochemical purity by radio-iTLC, showing >99.5% radiochemical purity after purification by PD10 column (free ^{89}Zr elutes at ~100-125 mm); (B) binding assay comparing modified DFO-AMG102 to unmodified AMG102; (C) western blot results from MET/HGF producing U87MG cells, MET producing MKN45 cells, SKOV3 ovarian cancer cells for reference, and LNCAP cells as a low MET expressing reference; and (D) results from an ELISA assay for human HGF showing the amount of HGF produced by select cell lines in spent media.

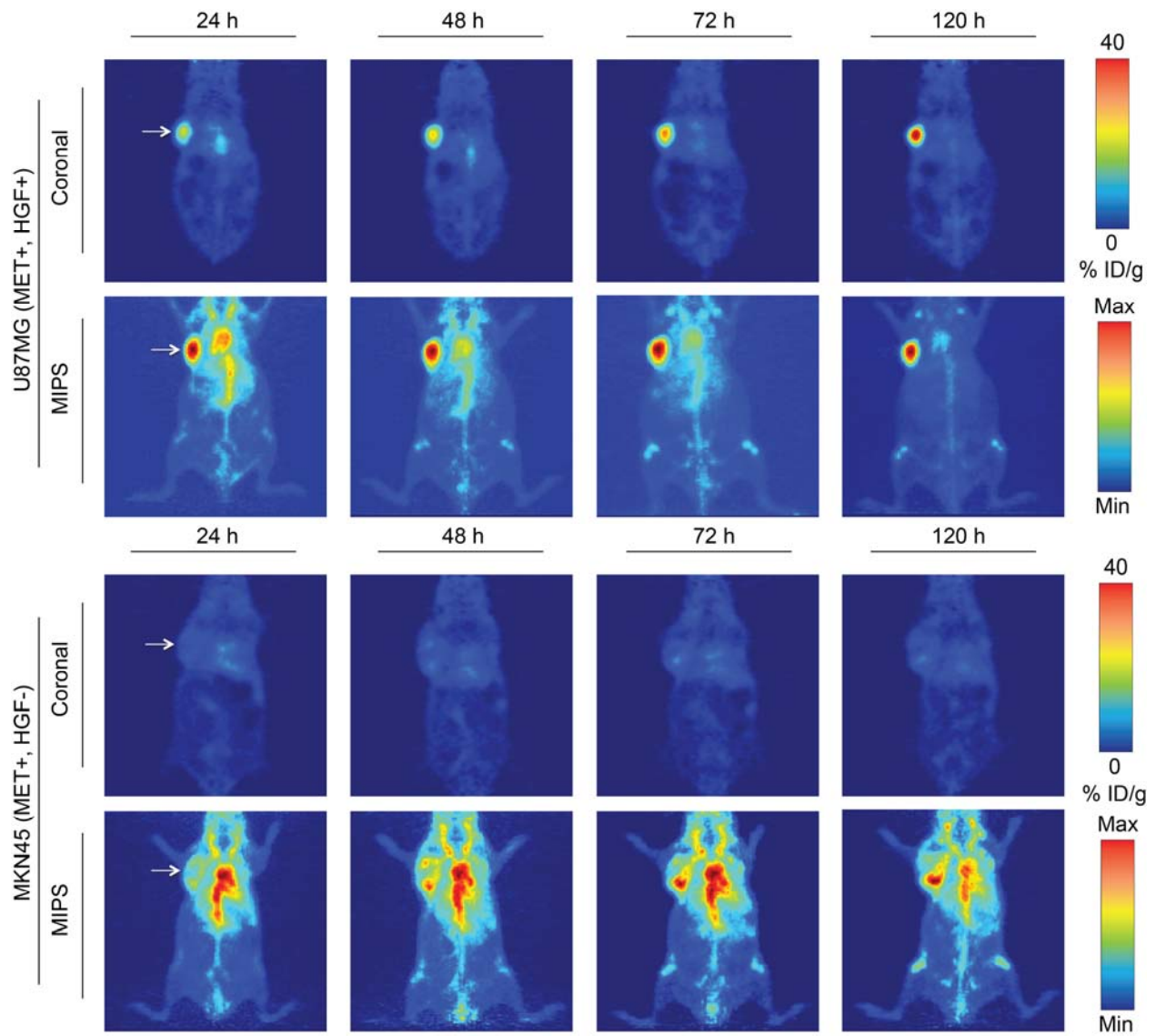
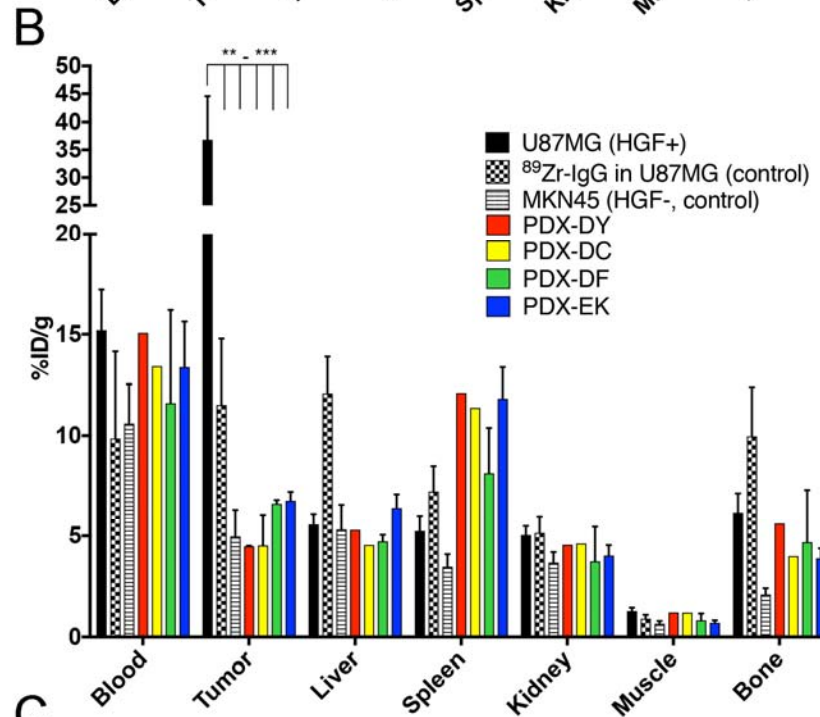
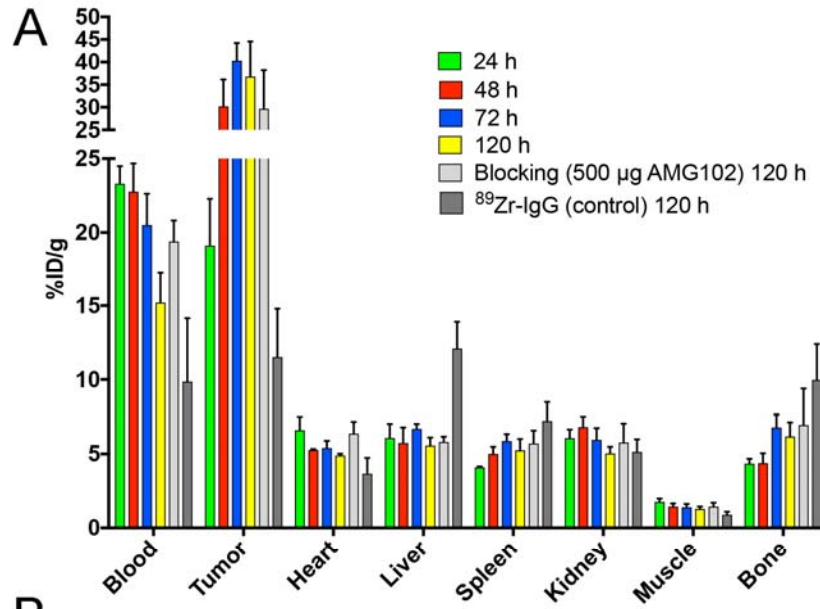


Fig. 4. Serial PET imaging of ^{89}Zr -DFO-AMG102 in positive (U87MG HGF+, MET+) and negative (MKN45 HGF-, MET+) mouse xenografts ($\sim 30\ \mu\text{g}$, $\sim 130\text{-}150\ \mu\text{Ci}$, $\sim 4.8\text{-}5.6\ \text{MBq}$, $200\ \mu\text{L}$ sterile saline), showing selective and high uptake in tumors that possess high *local HGF protein levels* (U87MG, $\sim 40\ \text{\%ID/g}$) and low uptake in tumors with low HGF levels (MKN45, $\sim 5\text{-}10\ \text{\%ID/g}$, EPR uptake only).



C

| Tumors | HGF in tumors (pg/mL)* | HGF in tumors (ng/mg of protein)* | HGF in blood serum (pg/mL) | ⁸⁹ Zr-DFO-AMG102 uptake in vivo (%ID/g) |
|--------|------------------------|-----------------------------------|----------------------------|--|
| U87MG | 6,627 | 3.31 | n.d. | 36.8 ± 7.8 |
| MKN45 | 189 | 0.09 | n.d. | 5.0 ± 1.3 |
| DY | 303 | 0.15 | n.d. | 4.5 ± 0.1 |
| DC | 217 | 0.11 | n.d. | 4.5 ± 1.6 |
| DF | 517 | 0.26 | n.d. | 6.6 ± 0.2 |
| EK | 46 | 0.02 | n.d. | 6.8 ± 0.4 |

*HGF-ELISA for tumors samples from subcutaneous mouse xenografts normalized to 100 µg of protein per well (2,100 µg/mL stocks)

Fig. 5. (A) Biodistribution data from ^{89}Zr -DFO-AMG102 in female nude mice bearing U87MG subcutaneous xenografts from 24-120 h post injection (~ 20 - $30 \mu\text{Ci}$, ~ 0.74 - 1.11 MBq , $\sim 5 \mu\text{g}$), including controls of ^{89}Zr -IgG (non-specific human IgG antibody) and a blocking dose (500 μg , 100 fold “cold” AMG102 co-injected), showing substantial uptake in U87MG tumors with high local levels of HGF, low uptake of the control ^{89}Zr -DFO-IgG (EPR effect), and no apparent blocking effect (see discussion); (B) Biodistribution data at 120 h p.i. showing ^{89}Zr -DFO-AMG102 and ^{89}Zr -DFO-IgG (control) (~ 20 - $30 \mu\text{Ci}$, ~ 0.74 - 1.11 MBq , $\sim 5 \mu\text{g}$) in U87MG (HGF+, MET+) and MKN45 (control, HGF-, MET+), and data from 4 different gastric PDXs at 120 h p.i. showing low tracer uptake from the ^{89}Zr -DFO-IgG control in U87MG and ^{89}Zr -DFO-AMG102 in MKN45, and similarly low uptake of ^{89}Zr -DFO-AMG102 in the 4 PDX models (HGF levels previously unknown); (C) data from ELISA assay for human HGF (pg/mL), and normalized HGF levels (ng/mg of protein) showing HGF levels in tumor homogenates and blood serum samples of tumor-bearing mice and corresponding *in vivo* %ID/g uptake values of ^{89}Zr -DFO-AMG102. Statistical significance shown from students unpaired t-test using PRISM software, * $p \leq 0.05$ ** = ≤ 0.01 *** = ≤ 0.001 , with all tumor uptake comparisons to U87MG having statistical significance between **-***.

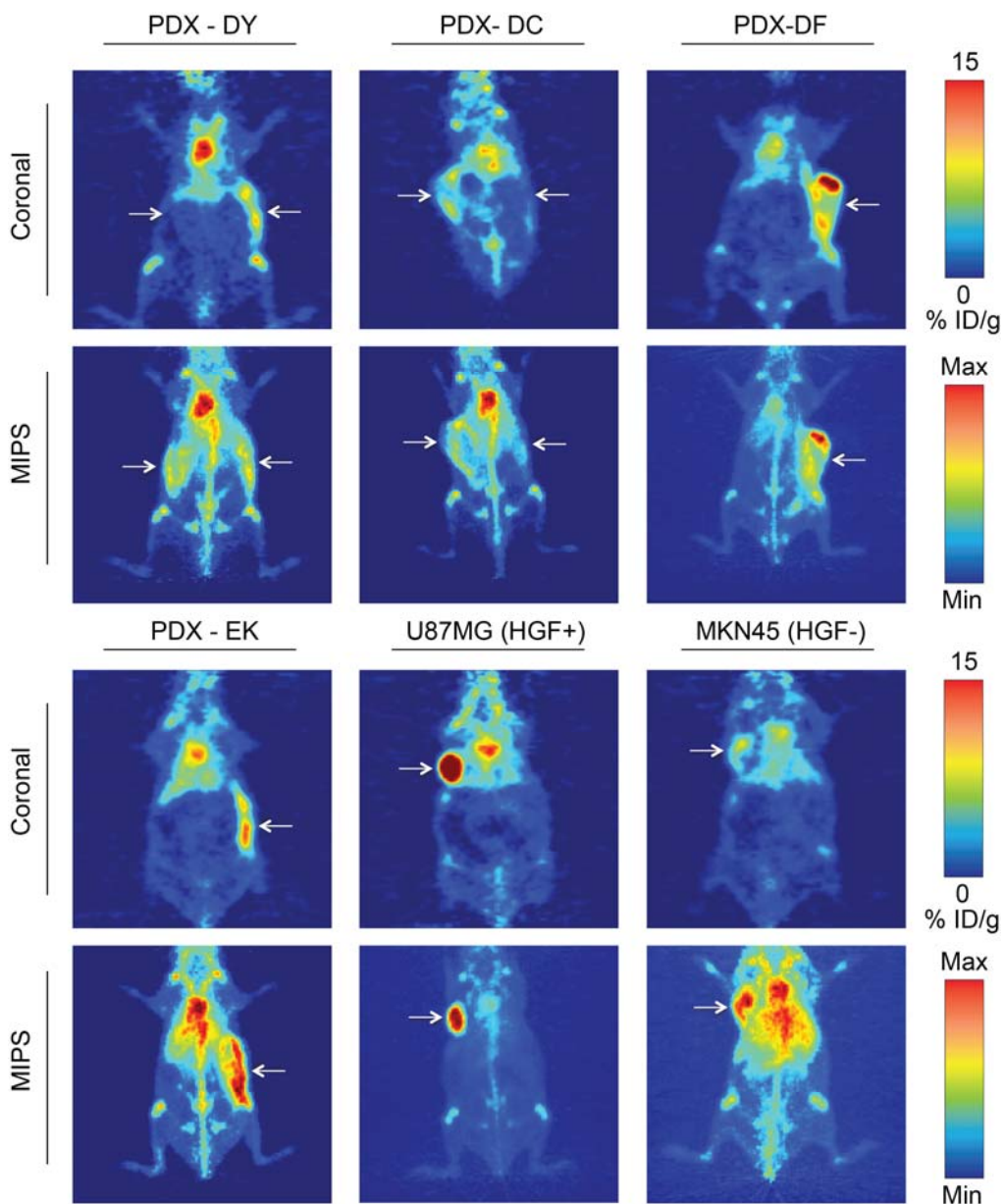


Fig. 6. ^{89}Zr -DFO-AMG102 ($\sim 30 \mu\text{g}$, $\sim 130\text{-}150 \mu\text{Ci}$, $\sim 4.8\text{-}5.6 \text{ MBq}$, $200 \mu\text{L}$ sterile saline) PET images 120 h p.i. comparing uptake in different tumor types, showing high uptake in HGF+ U87MG tumors ($\sim 40\%$ ID/g), and low uptake in HGF- MKN45 tumors ($\sim 5\text{-}10\%$ ID/g). Mice bearing gastric PDXs (DY, DC, DF, EK) with previously unknown levels of HGF show similarly low uptake to the HGF- MKN45 xenografts, non-invasively determining little or no HGF present. Tumors are highlighted with white arrows, and images with two arrows indicate bilateral xenografts (DY, DC), full serial-PET images in Supplemental Figs. 8-9.

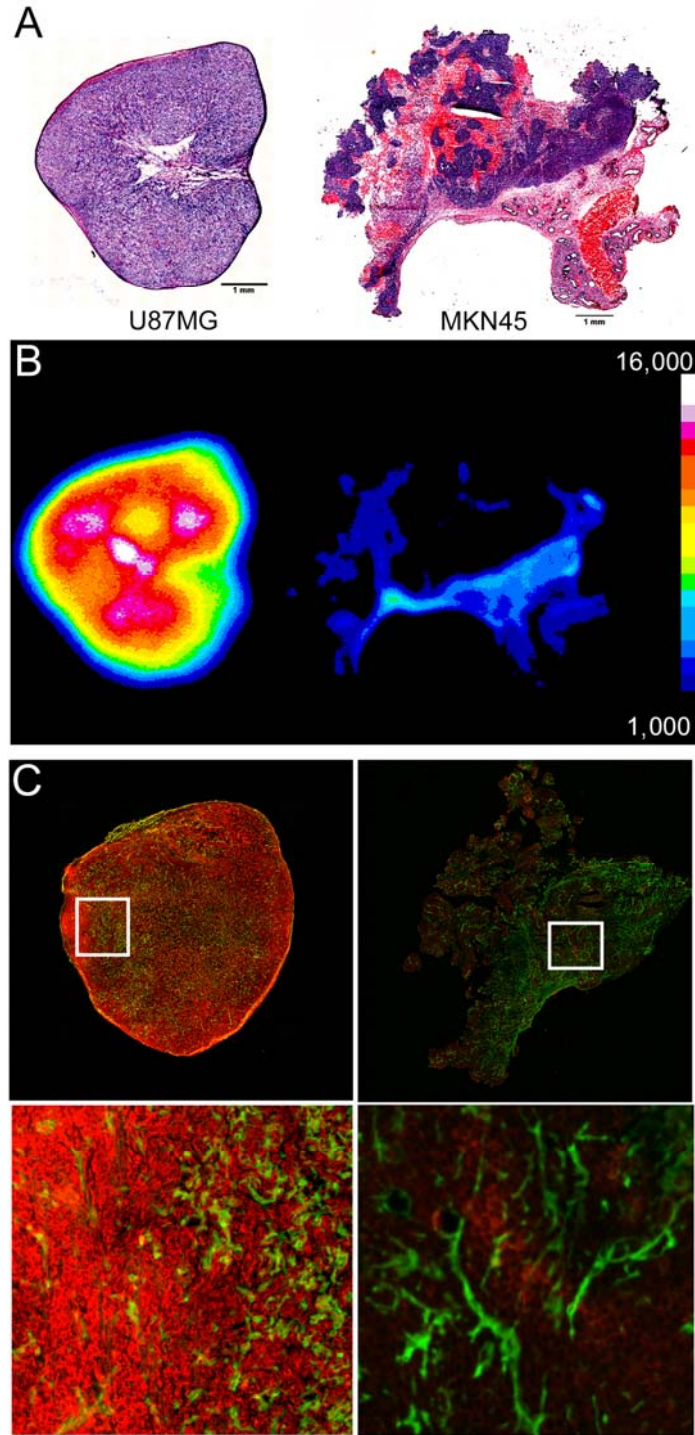


Fig. 7. Sections of tumors obtained at time of necropsy following PET, showing A) hematoxylin and eosin staining (U87MG left, MKN45 right), B) autoradiography U87MG left (high uptake) and MKN45 right (low uptake), and C) immunofluorescence staining shown in green for perlecan (extracellular matrix/stroma) and red for anti-HGF (U87MG left, MKN45 right), confirming high concentrations of HGF protein only in U87MG tumors.

SUPPORTING INFORMATION

Evaluation of Clinical Patient Data. Raw patient data was obtained from the TCGA Research Network and parsed using an in-house MATLAB script. Level 3 reverse phase protein array data was used to stratify the stomach adenocarcinoma cohort into quantiles of protein expression levels and the survival time of each individual was determined using Clinical Biotab data. Each quantile is represented in a Kaplan-Meier survival curve, and this analysis was performed for phosphorylated-MET and overall MET protein expression. Level 3 Agilent G4502A gene expression microarray data was used to generate MET and HGF RNA expression box-plots. The cancer types used in these plots were selected based on the availability of Level 3 Agilent G4502A gene expression microarray data in the TCGA database. The survival curves and box-plots were generated using GraphPad Prism version 6.0f for Mac OS X (GraphPad Software, La Jolla California USA, www.graphpad.com). The results shown and discussed here are in whole or part based upon data generated by the TCGA Research Network: <http://cancergenome.nih.gov/>.

Antibody Modification. AMG102 (lot #067A32374, obtained from Amgen Inc., Thousand Oaks, CA) and a non-specific human IgG antibody (from human serum, Sigma Aldrich) was purified using PD10 size-exclusion columns (PD10, Sephadex G-25 M, PD10 column, GE Healthcare, PBS pH 7.4, 3 times), followed by centrifugal filter units (Amicon® ultra centrifuge filters, Ultracel®-50: regenerated cellulose, Millipore Corp., Billerica, MA) (PBS, pH 7.4) to remove additives. After purification, the antibody (PBS pH 7.4) was kept in the fridge at 4 °C as a stock solution (~5-10 mg/mL). Subsequently, aliquots of each antibody solution (3.0 mg antibody) were combined with PBS (up to 1000 µL total, pH 7.4), the pH of the resulting solution was adjusted to 8.8-9.0 with 0.1 M Na₂CO₃ (~30 µL), and 5 equivalents of *p*-SCN-Bn-DFO (Macrocyclics, Inc. Dallas, TX)

was added in 10-15 μL DMSO. The reactions were incubated at 37 $^{\circ}\text{C}$ for 1 h, followed by PD10 purification and centrifugal filtration (Amicon 50 kDa) to purify the resultant antibody conjugate. The final immunoconjugate stock solutions were stored in PBS (pH 7.4) at 4 $^{\circ}\text{C}$.

MALDI-TOF MS/MS Analysis to Determine the Number of Chelates per Antibody.

The number of benzylthiourea-linked desferrioxamine (DFO) chelates conjugated to AMG102 was determined using MALDI-TOF MS/MS (Alberta Proteomics and Mass Spectrometry Facility, University of Alberta, Canada). All experiments were performed in triplicate, and all samples were run along with standard samples of unmodified AMG102 (run on the same day). 1 μL of each sample (1 mg/mL) was mixed with 1 μL of sinapic acid (10 mg/ml in 50% acetonitrile:water and 0.1% trifluoroacetic acid). 1 μL of the sample/ matrix solution was then spotted onto a stainless steel target plate and allowed to air dry. All mass spectra were obtained using a Bruker Ultraflex MALDI-TOF/TOF (Bruker Daltonic GmbH). Ions were analyzed in positive mode, and external calibration was performed using a standard protein mixture (Bovine Serum Albumin). The mass signals ($M^{+2}/2$) at half of the parent molecular weight of the antibody were taken from each chromatogram and averaged ($n = 3$), and the average unmodified AMG102 weight was subtracted from the modified antibody weight to determine the mass contribution from conjugated chelator. The mass difference was divided by the molecular weight of the attached bifunctional chelator (*p*-SCN-Bn-DFO), and the error in each triplicate set of measurements (unmodified AMG102 vs modified AMG102) was propagated to the final value of the number of chelates per antibody. Full MALDI-TOF spectra are shown in Supplementary Figs. 1-6.

Determination of Antibody Binding Affinity. The immunoreactivity of ^{89}Zr -DFO-

AMG102 could not be determined from typically utilized specific radioactive cellular-binding assays due to HGF not being cell-bound. In place of typical cell-binding assays, Immulon 2HB high binding 96 well plates were coated with human HGF (HGF Recombinant Human Protein, Life Technologies) by adding 100 μ L of an HGF solution in PBS (0.2 μ g/mL, 200 ng/mL) and mixing overnight at 4 °C. HGF coated plates were aspirated/rinsed 3 times with PBS/0.2% tween (PBST). HGF coated plates were then blocked with 100 μ L of 3% BSA-PBS for 1 hr at RT. Blocking solution was aspirated/rinsed 3 times with PBST. Samples of unmodified AMG102 and the immunoconjugate DFO-AMG102 (60 μ g/mL) were added to the first wells (125 μ L), and a serial dilution (1/5, 25 μ L transferred from each well, leaving a total of 100 μ L per well) was performed 11 times, yielding wells with concentrations from 60 – 1 x 10⁻⁶ μ g/mL in 100 μ L total volume in each well. A nonspecific human IgG isotype antibody was also used as a control for non-specific binding. Antibody solutions were allowed to sit for 1 hr at RT. Plates were washed 3 times with PBST, followed by adding 100 μ L of rabbit anti human HRP secondary antibody (1/130000 dilution, from 2 mg/mL stock, ab6759 abcam) and incubating for 1 hr at RT. The plates were then aspirated/rinsed 3 times with PBST, followed by enzymatic reaction detections by addition of a 1:1 mixture of peroxidase substrate solution B and TMB peroxidase substrate (100 μ L per well, KPL TMB microwell peroxidase substrate system) and incubating for 10 min at RT. Development was stopped by addition of H₂SO₄ (0.1 M, 100 μ L per well). Plates were read at 450 nM on a Molecular Devices SpectraMax M5 plate reader. Data was plotted and analyzed in PRISM software to determine EC50 values.

ELISA Assay for HGF Protein Levels in Spent Media, Serum, and Tumor Homogenates. ELISA assay kits for detecting human HGF were obtained from Life Technologies (Novex, KAC2211). For cell media, spent media was harvested after 5

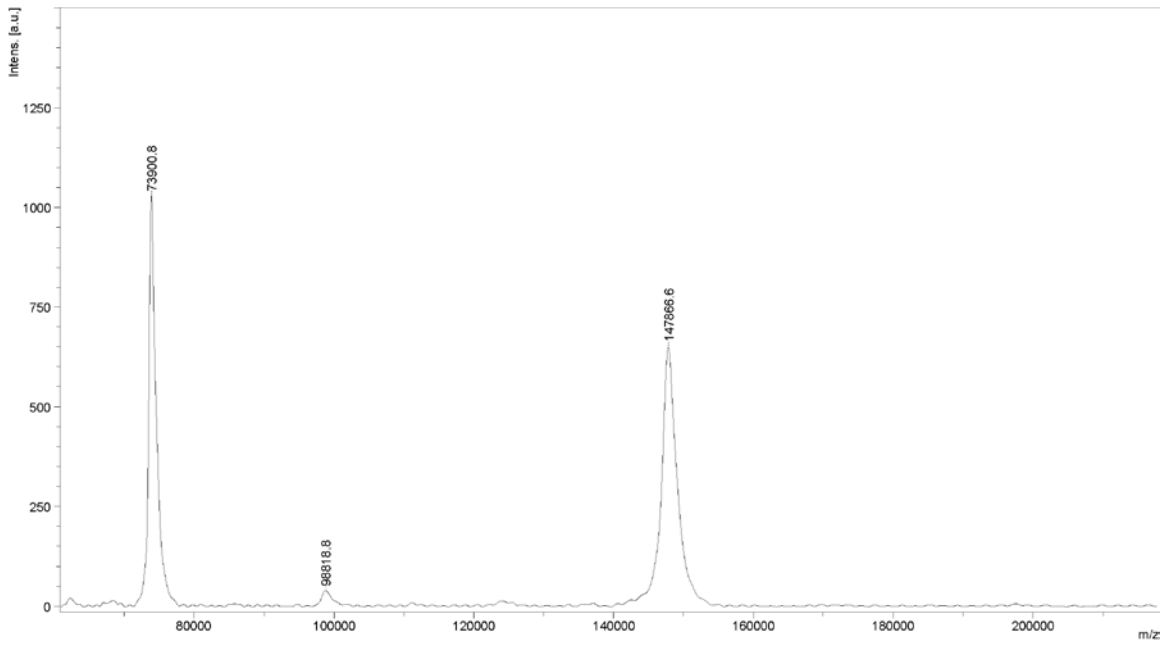
days of incubation, and media was analyzed by the ELISA kits with concentrations of 1:1, 1:5, 1:10, and 1:100. HGF protein could only be detected in the 1:1 concentration of spent U87MG cell media. For serum samples of U87MG, MKN45, and PDX tumor bearing mice, blood was obtained either by retro-orbital bleed or by terminal cardiac puncture (no heparin was added due to ELISA interference). Blood was allowed to sit on ice for 30 minutes, and was then centrifuged at 600 g for 15 minutes to separate blood cells and clotting factors. The straw-colored blood serum was decanted by pipet, and was analyzed by ELISA kit in concentrations of 1:1, 1:10, and 1:100. Tumor samples were homogenized by taking a solid piece of tumor and adding 250 μ L of RIPA buffer, 2.5 μ L of protease inhibitor cocktail (abcam), mechanically homogenizing, sonication, and then centrifugation to remove debris. Tumor homogenates were normalized for protein concentration using a BCA assay to 100 μ g of protein per well.

Western Blot Analysis of Cell Lines for MET Expression. For immunoblot assays, cells were harvested and cell pellets were resuspended in RIPA buffer with protease and phosphatase inhibitor cocktails (Calbiochem) and sonicated. After protein quantification, lysates were run on 7% precast NuPAGE Tris-Acetate gels (ThermoFischer Scientific), transferred to Immobilon-P PVDF membrane (EMD Millipore), blocked in 7% non-fat milk (Carnation), incubated in primary antibody solution for 1 hour at room temperature, washed, incubated in secondary antibody solution for 30 minutes at room temperature, washed, and exposed. Antibodies were used at the following concentrations in TBS-T to probe the blots: 1:5000 MET (Anti-Met (c-Met) antibody [EP1454Y] ab51067), 1:20,000 actin. Appropriate secondary antibodies were used at 1:5000 for MET (rabbit anti human HRP, abcam) and 1:7500 for actin. Chemiluminescence was used to visualize protein expression with ECL on film (Amersham ECL Prime, GE Healthcare).

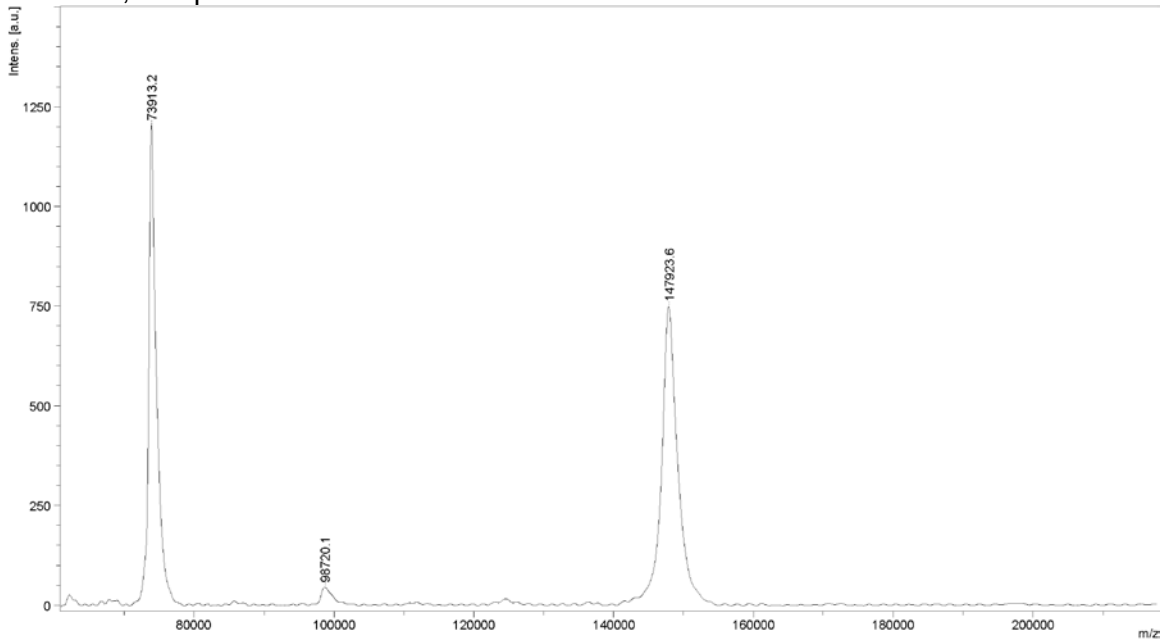
Cell Culture. Flasks containing cells were stored in cell incubators maintained at 37 °C and a 5% CO₂ concentration. Cell lines were harvested weekly using a formulation of 0.25% trypsin/0.53 mM EDTA in Hank's Buffered Salt Solution without calcium and magnesium, which was then neutralized with at least 200% the volume of trypsin with the appropriate medium containing fetal bovine serum.

The human ovarian cancer cell line SKOV3 (cultured in McCoy's 5A Medium, modified to contain 1.5 mM L-glutamine and 2200 mg/L sodium bicarbonate), human glioblastoma cell line U87MG (cultured in Dulbecco's Modified Eagle's Medium, 2mM L-Glutamine, 1500mg/L Sodium Bicarbonate), human gastric carcinoma cell line Kato III (cultured in Iscove's Modified Dulbecco's Medium (IMDM) containing 4 mM L-glutamine, 4500 mg/L glucose, and 1500 mg/L sodium bicarbonate), and human gastric cancer cell line NCI-N87 (cultured in RPMI-1640 medium modified to contain 2 mM L-glutamine, 10 mM HEPES, 1 mM sodium pyruvate, 4500 mg/L glucose, and 1500 mg/L sodium bicarbonate) were all grown with 100 units/mL penicillin G and 100 µg/mL streptomycin and 10% fetal bovine serum, and were purchased from American Type Culture Collection (ATCC, Manassas, VA).

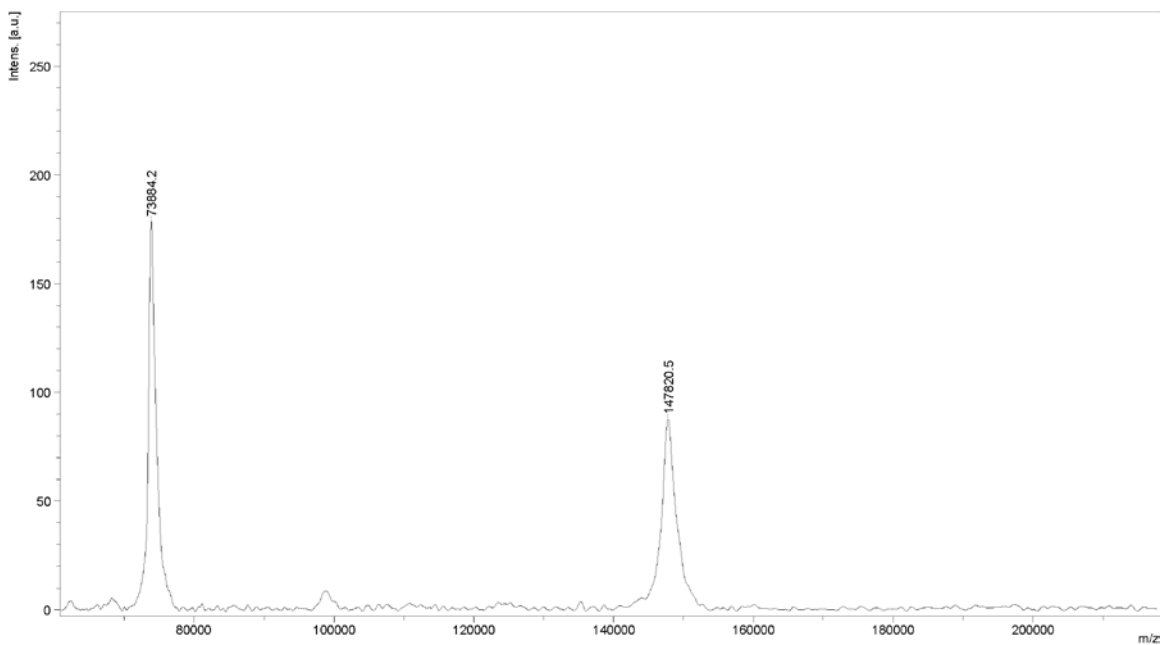
The human gastric cancer cell line MKN45 (cultured in RPMI-1640 medium modified to contain 2 mM L-glutamine, and 1500 mg/L sodium bicarbonate) and human gastric carcinoma cell line GTL-16 (cultured in Dulbecco's modified Eagle's high glucose Medium, 2 mM L-glutamine) were grown with 10% fetal bovine serum, 100 units/mL penicillin G and 100 µg/mL streptomycin, and were obtained from Dr. Martin R. Weiser's lab at MSKCC.



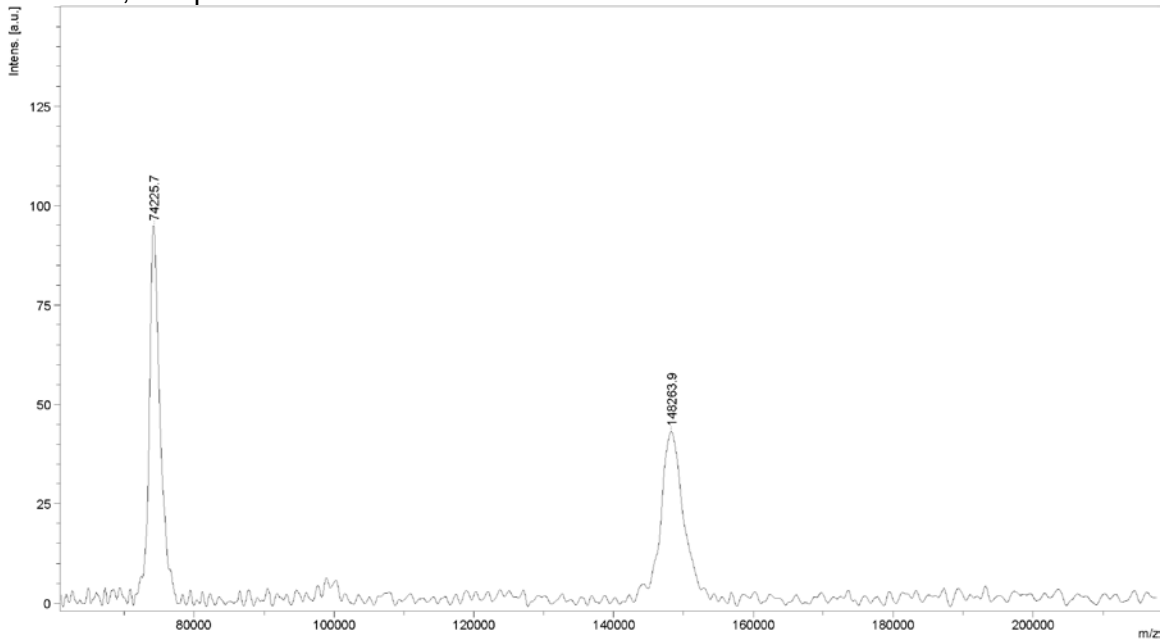
Supplemental Fig. 1. MALDI-TOF MS/MS mass spectrometry analysis of unmodified AMG102, sample #1.



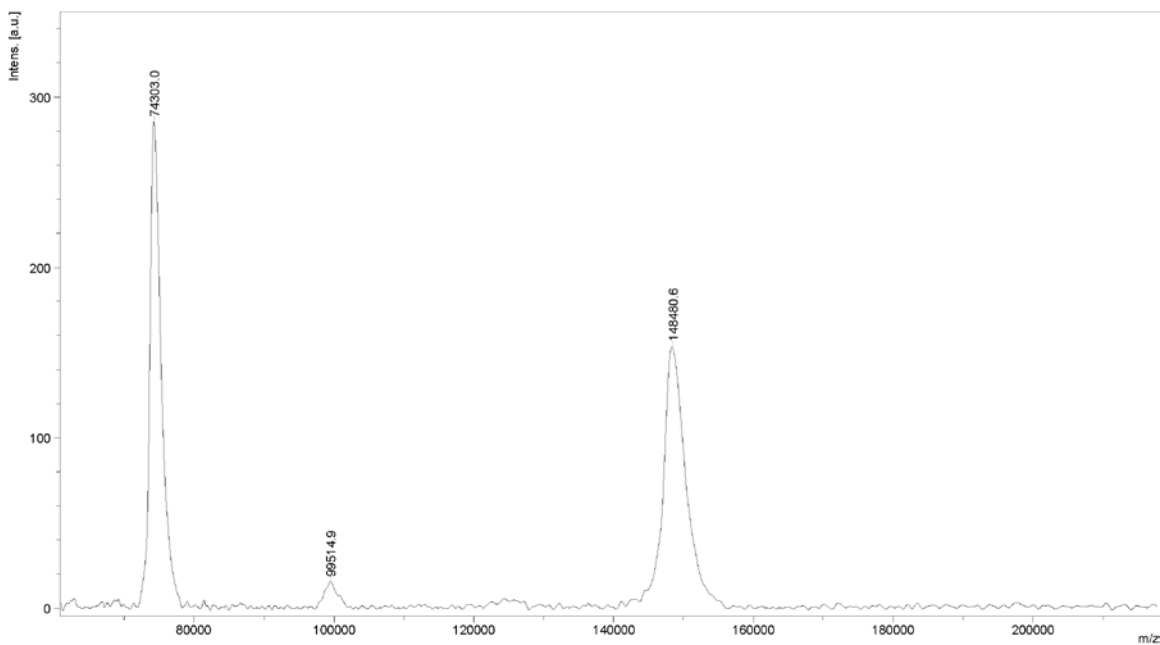
Supplemental Fig. 2. MALDI-TOF MS/MS mass spectrometry analysis of unmodified AMG102, sample #2.



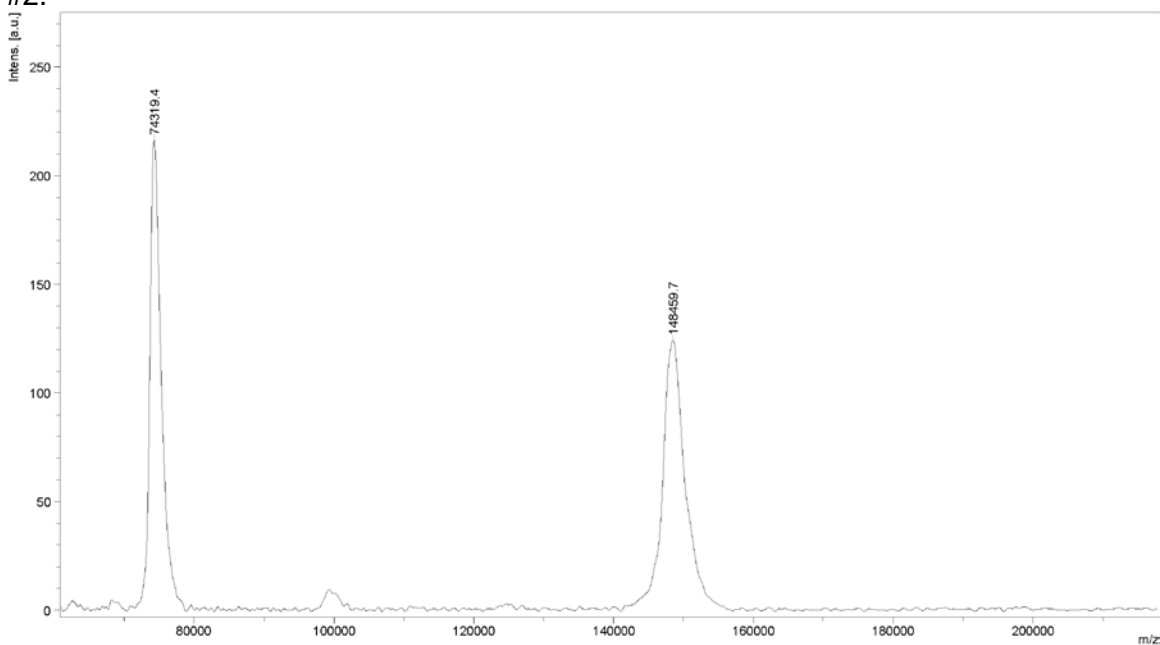
Supplemental Fig. 3. MALDI-TOF MS/MS mass spectrometry analysis of unmodified AMG102, sample #3.



Supplemental Fig. 4. MALDI-TOF MS/MS mass spectrometry analysis of AMG102 that had been reacted with 5 equivalents of *p*-SCN-Bn-DFO to form DFO-AMG102, sample #1.



Supplemental Fig. 5. MALDI-TOF MS/MS mass spectrometry analysis of AMG102 that had been reacted with 5 equivalents of *p*-SCN-Bn-DFO to form DFO-AMG102, sample #2.



Supplemental Fig. 6. MALDI-TOF MS/MS mass spectrometry analysis of AMG102 that had been reacted with 5 equivalents of *p*-SCN-Bn-DFO to form DFO-AMG102, sample #3.

Supplemental Table 1. MALDI-TOF MS/MS results of AMG102 and AMG102-DFO, submitted as 1 µg/µL solutions, 10 µL total, analyzed by the University of Alberta Mass Spectrometry Facility, with mass units as daltons (Da).

| | AMG102 standard | | AMG102 DFO | |
|-------------------|-----------------|-----------|------------|-----------|
| | (m+2/2) | Full mass | (m+2/2) | Full mass |
| Mass (Da) | 73900.8 | 147801.6 | 74225.7 | 148451.4 |
| Mass (Da) | 73913.2 | 147826.4 | 74303.0 | 148606.0 |
| Mass (Da) | 73884.2 | 147768.4 | 74319.4 | 148638.8 |
| Average Mass (Da) | 73899.4 | 147798.8 | 74282.7 | 148565.4 |
| Std. Dev (Da) | 14.6 | 29.1 | 50.0 | 100.1 |

| Immunoconjugate | Mass difference (Da) | Chelate mass (Da) | Chelates/antibody average | Standard Deviation |
|-----------------|----------------------|-------------------|---------------------------|--------------------|
| AMG102-DFO | 766.6 | 752.9 | 1.0 | 0.1 |

Supplemental Table 2. Biodistribution data of ⁸⁹Zr-DFO-AMG102 or ⁸⁹Zr-DFO-IgG (as indicated in table) (~20-30 µCi, 0.74-1.1 MBq, ~5 µg, in 200-250 µL of sterile saline; tumor volume ~ 100-150 mm³) in female nude athymic mice bearing subcutaneous xenografts of U87MG or MKN45 (as indicated in table).

| ⁸⁹ Zr-DFO-antibody | AMG102 | | | AMG102 | | | AMG102 | | |
|-------------------------------|--------|-----------|---|--------|-----------|---|--------|-----------|---|
| | U87MG | | | U87MG | | | U87MG | | |
| Biodistribution time | 24 h | | | 48 h | | | 72 h | | |
| Organ | %ID/g | Std. Dev. | n | %ID/g | Std. Dev. | n | %ID/g | Std. Dev. | n |
| Blood | 23.3 | 1.2 | 5 | 22.8 | 1.9 | 5 | 20.5 | 2.1 | 5 |
| Tumor | 19.1 | 3.2 | 5 | 30.2 | 5.9 | 5 | 40.3 | 3.9 | 5 |
| Heart | 6.6 | 0.9 | 5 | 5.3 | 0.1 | 5 | 5.4 | 0.5 | 5 |
| Lungs | 9.3 | 2.0 | 5 | 10.4 | 1.4 | 5 | 11.2 | 1.5 | 5 |
| Liver | 6.1 | 1.0 | 5 | 5.7 | 1.1 | 5 | 6.7 | 0.3 | 5 |
| Spleen | 4.1 | 0.1 | 5 | 5.0 | 0.5 | 5 | 5.9 | 0.5 | 5 |
| Pancreas | 2.1 | 0.3 | 5 | 2.1 | 0.4 | 5 | 2.0 | 0.2 | 5 |
| Stomach | 1.6 | 0.4 | 5 | 1.7 | 0.6 | 5 | 1.2 | 0.5 | 5 |
| Small Intestine | 2.1 | 0.2 | 5 | 2.4 | 0.5 | 5 | 2.1 | 0.3 | 5 |
| Large Intestine | 1.2 | 0.3 | 5 | 1.3 | 0.3 | 5 | 1.0 | 0.2 | 5 |
| Kidney | 6.1 | 0.6 | 5 | 6.8 | 0.7 | 5 | 6.0 | 0.8 | 5 |
| Muscle | 1.8 | 0.2 | 5 | 1.5 | 0.2 | 5 | 1.4 | 0.2 | 5 |
| Bone | 4.4 | 0.3 | 5 | 4.4 | 0.7 | 5 | 6.8 | 0.9 | 5 |
| Skin | 6.9 | 1.4 | 5 | 5.0 | 0.6 | 5 | 7.7 | 0.3 | 5 |

Supplemental Table 3. Biodistribution data of ⁸⁹Zr-DFO-AMG102 or ⁸⁹Zr-DFO-IgG (as indicated in table) (~20-30 μ Ci, 0.74-1.1 MBq, ~5 μ g, in 200-250 μ L of sterile saline; tumor volume ~ 100-150 mm³) in female nude athymic mice bearing subcutaneous xenografts of U87MG or MKN45 (as indicated in table).

| ⁸⁹ Zr-DFO-antibody Tumor or xenograft | AMG102 | | | AMG102 + blocking (500 μ g AMG102) | | | Human IgG | | | AMG102 | | |
|---|--------|-----------|---|---|-----------|---|-----------|-----------|---|--------|-----------|----|
| | U87MG | | | U87MG | | | U87MG | | | MKN45 | | |
| Biodistribution time | 120 h | | | 120 h | | | 120 h | | | 120 h | | |
| Organ | %ID/g | Std. Dev. | n | %ID/g | Std. Dev. | n | %ID/g | Std. Dev. | n | %ID/g | Std. Dev. | n |
| Blood | 15.2 | 2.0 | 5 | 19.4 | 1.4 | 5 | 9.9 | 4.3 | 5 | 10.6 | 1.9 | 10 |
| Tumor | 36.8 | 7.8 | 5 | 29.7 | 8.6 | 5 | 11.5 | 3.3 | 5 | 5.0 | 1.3 | 10 |
| Heart | 4.9 | 0.1 | 5 | 6.4 | 0.8 | 5 | 3.7 | 1.1 | 5 | 2.7 | 0.5 | 10 |
| Lungs | 8.3 | 1.8 | 5 | 10.4 | 1.6 | 5 | 5.7 | 1.8 | 5 | 5.9 | 1.0 | 10 |
| Liver | 5.6 | 0.5 | 5 | 5.8 | 0.4 | 5 | 12.1 | 1.8 | 5 | 5.3 | 1.2 | 10 |
| Spleen | 5.3 | 0.8 | 5 | 5.7 | 0.9 | 5 | 7.2 | 1.3 | 5 | 3.5 | 0.6 | 10 |
| Pancreas | 1.9 | 0.3 | 5 | 2.0 | 0.3 | 5 | 1.3 | 0.3 | 5 | 1.0 | 0.2 | 10 |
| Stomach | 1.4 | 0.2 | 5 | 1.7 | 0.4 | 5 | 1.2 | 0.2 | 5 | 0.8 | 0.3 | 10 |
| Small Intestine | 1.4 | 0.1 | 5 | 1.7 | 0.1 | 5 | 1.3 | 0.2 | 5 | 0.9 | 0.2 | 10 |
| Large Intestine | 0.8 | 0.1 | 5 | 0.8 | 0.1 | 5 | 0.6 | 0.1 | 5 | 0.7 | 0.2 | 10 |
| Kidney | 5.0 | 0.5 | 5 | 5.8 | 1.3 | 5 | 5.2 | 0.8 | 5 | 3.7 | 0.5 | 10 |
| Muscle | 1.3 | 0.2 | 5 | 1.5 | 0.3 | 5 | 0.9 | 0.2 | 5 | 0.7 | 0.1 | 10 |
| Bone | 6.2 | 1.0 | 5 | 7.0 | 2.4 | 5 | 10.0 | 2.4 | 5 | 2.1 | 0.3 | 10 |
| Skin | 5.4 | 1.2 | 5 | 5.9 | 0.5 | 5 | 4.4 | 0.3 | 5 | 4.8 | 1.1 | 10 |

Supplemental Table 4. Biodistribution data displayed as %ID of ⁸⁹Zr-DFO-AMG102 (~20-30 μ Ci, 0.74-1.1 MBq, ~5 μ g, in 200-250 μ L of sterile saline; tumor volume ~ 100-150 mm³) in female nude athymic mice bearing subcutaneous xenografts of U87MG, with data displayed as %ID to properly highlight blocking efficacy, due to dramatic tumor shrinkage observed in the blocking group.

| Organ | U87MG, ⁸⁹ Zr-DFO-AMG102, 120 h | | | U87MG, ⁸⁹ Zr-DFO-AMG102, 500 μ g block, 120 h | | |
|-----------------|---|-----------|---|--|-----------|---|
| | %ID | Std. Dev. | n | %ID | Std. Dev. | n |
| Blood | 7.7 | 2.1 | 5 | 10.6 | 3.1 | 5 |
| Tumor | 8.1 | 3.7 | 5 | 1.9 | 1.3 | 5 |
| Heart | 0.6 | 0.1 | 5 | 0.8 | 0.2 | 5 |
| Lungs | 1.6 | 0.5 | 5 | 2.0 | 0.2 | 5 |
| Liver | 5.2 | 0.5 | 5 | 6.0 | 0.8 | 5 |
| Spleen | 0.6 | 0.1 | 5 | 0.5 | 0.1 | 5 |
| Pancreas | 0.4 | 0.04 | 5 | 0.3 | 0.1 | 5 |
| Stomach | 0.5 | 0.1 | 5 | 0.6 | 0.1 | 5 |
| Small Intestine | 2.2 | 0.1 | 5 | 2.5 | 0.4 | 5 |
| Large Intestine | 1.3 | 0.2 | 5 | 1.3 | 0.3 | 5 |
| Kidney | 2.2 | 0.2 | 5 | 2.3 | 0.5 | 5 |
| Muscle | 0.1 | 0.02 | 5 | 0.2 | 0.03 | 5 |
| Bone | 0.3 | 0.1 | 5 | 0.3 | 0.2 | 5 |
| Skin | 1.1 | 0.2 | 5 | 1.2 | 0.1 | 5 |

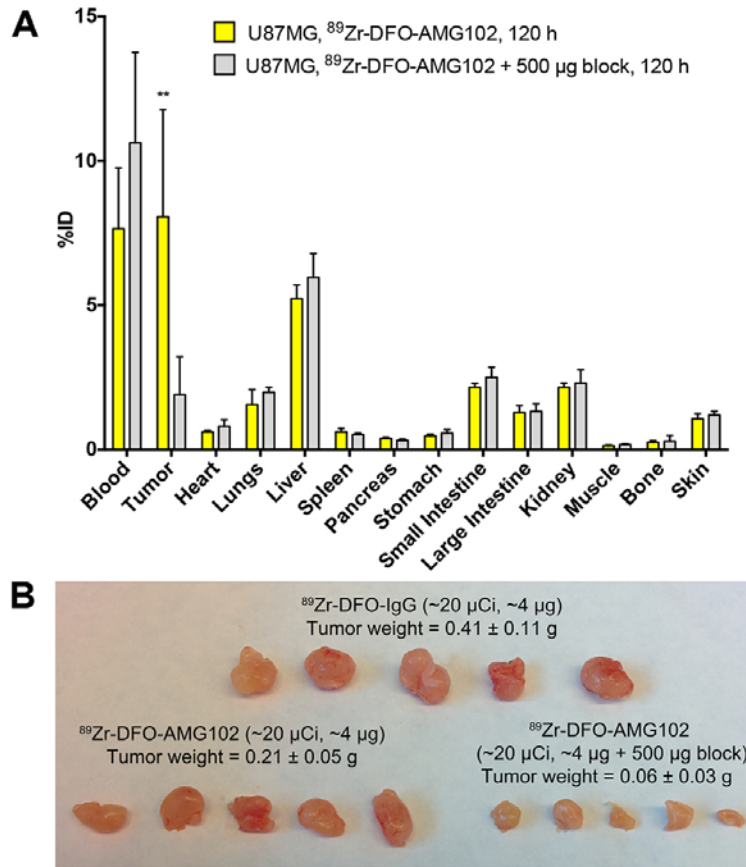
Supplemental Table 5. Biodistribution data shown as tumor/organ ratios of ⁸⁹Zr-DFO-AMG102 or ⁸⁹Zr-DFO-IgG (as indicated in table) (~20-30 μ Ci, 0.74-1.1 MBq, ~5 μ g, in 200-250 μ L of sterile saline; tumor volume ~ 100-150 mm³) in female nude athymic mice bearing subcutaneous xenografts of U87MG or MKN45.

| ⁸⁹ Zr-DFO-antibody | AMG102 | | | | | | |
|-------------------------------|--------|--------|--------|--------|--------------|-----------|--------|
| | AMG102 | AMG102 | AMG102 | AMG102 | AMG102 block | human IgG | AMG102 |
| Tumor xenograft | U87MG | U87MG | U87MG | U87MG | U87MG | U87MG | MKN45 |
| Biodistribution time | 24 h | 48 h | 72 h | 120 h | 120 h | 120 h | 120 h |
| Tumor / Blood ratio | 0.8 | 1.3 | 2.0 | 2.4 | 1.5 | 1.2 | 0.4 |
| Tumor / Heart ratio | 2.9 | 5.7 | 7.5 | 7.5 | 4.6 | 3.1 | 1.7 |
| Tumor / Lungs ratio | 2.1 | 2.9 | 3.6 | 4.4 | 2.9 | 2.0 | 0.9 |
| Tumor / Liver ratio | 3.1 | 5.3 | 6.0 | 6.6 | 5.1 | 1.0 | 1.0 |
| Tumor / Kidney ratio | 3.1 | 4.4 | 6.8 | 7.3 | 5.1 | 2.2 | 1.4 |
| Tumor / Bone ratio | 4.4 | 6.9 | 5.9 | 6.0 | 4.3 | 1.2 | 2.5 |

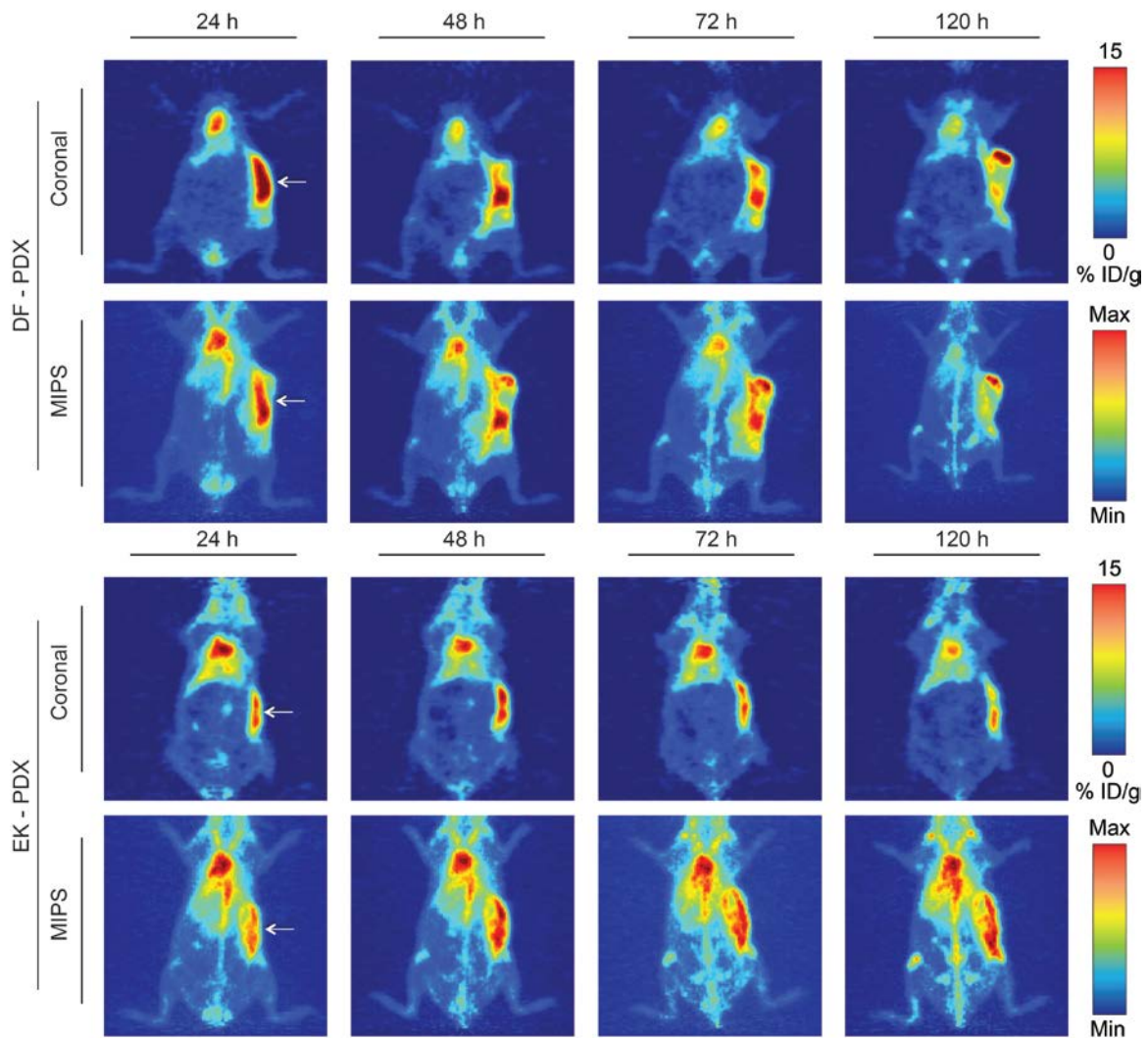
| Tumor / organ Std. Dev. | 24 h | 48 h | 72 h | 120 h | 120 h | 120 h | 120 h |
|-------------------------|------|------|------|-------|-------|-------|-------|
| Tumor / Blood ratio | 0.1 | 0.3 | 0.3 | 0.6 | 0.5 | 0.6 | 0.1 |
| Tumor / Heart ratio | 0.6 | 1.1 | 1.0 | 1.6 | 1.5 | 1.3 | 0.5 |
| Tumor / Lungs ratio | 0.6 | 0.7 | 0.6 | 1.4 | 0.9 | 0.9 | 0.3 |
| Tumor / Liver ratio | 0.7 | 1.4 | 0.6 | 1.5 | 1.5 | 0.3 | 0.4 |
| Tumor / Kidney ratio | 0.6 | 1.0 | 1.1 | 1.7 | 1.9 | 0.7 | 0.4 |
| Tumor / Bone ratio | 0.8 | 1.7 | 0.9 | 1.6 | 1.9 | 0.4 | 0.7 |

Supplemental Table 6. Biodistribution data of ⁸⁹Zr-DFO-AMG102 (~20-30 μCi, 0.74-1.1 MBq, ~5 μg, in 200-250 μL of sterile saline) post PET imaging at 120 h p.i. in patient-derived xenograft models (PDX) in female nude athymic mice bearing.

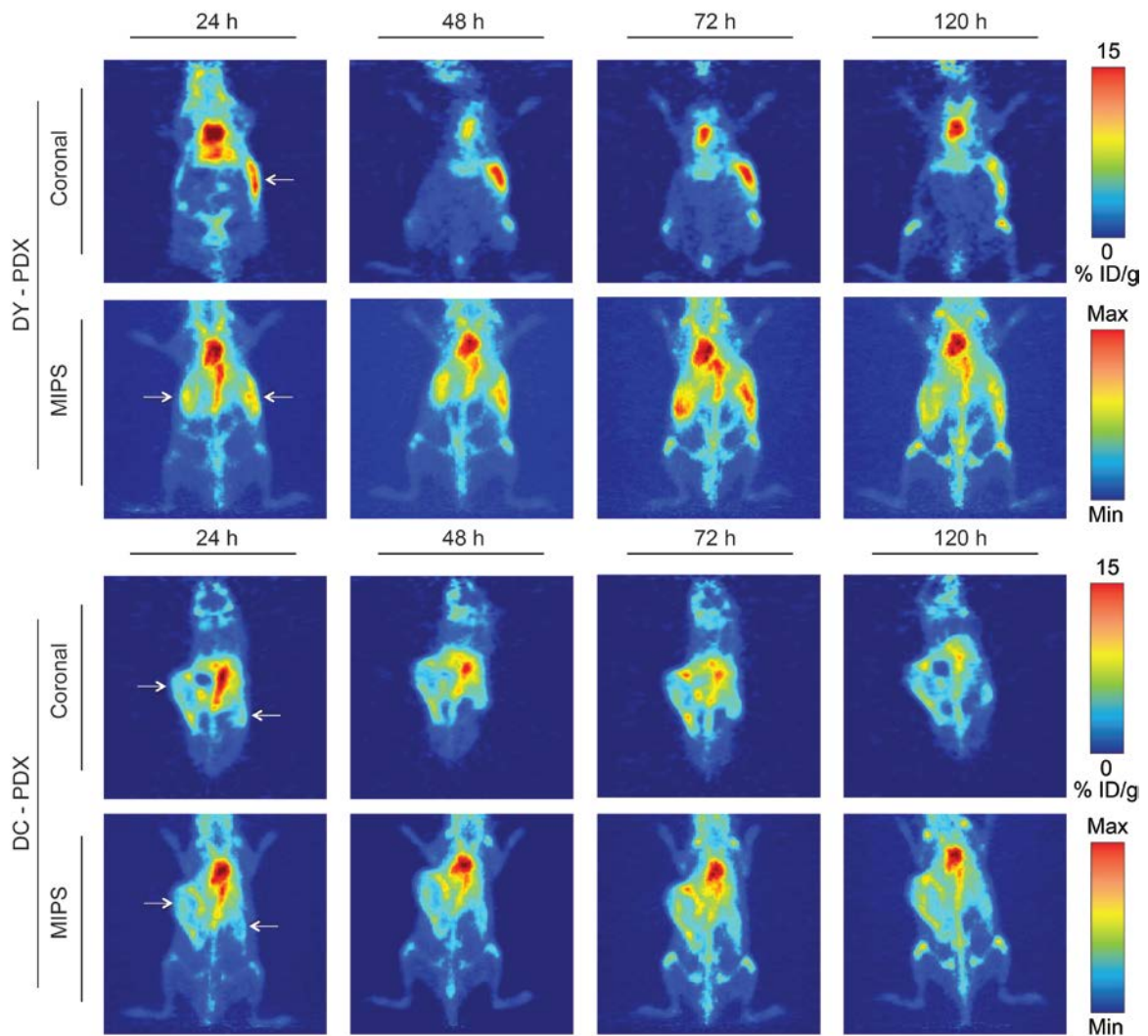
| Tumor xenograft | PDX-DY | | | PDX-DC | | | PDX-DF | | | PDX-EK | | |
|-----------------|--------|-------|-----------|--------|-------|-----------|--------|-------|-----------|--------|-------|-----------|
| | Organ | %ID/g | Std. Dev. | n | %ID/g | Std. Dev. | n | %ID/g | Std. Dev. | n | %ID/g | Std. Dev. |
| Blood | 15.1 | | 1 | 13.4 | | 1 | 11.6 | 4.6 | 2 | 13.4 | 2.3 | 3 |
| Tumor | 4.5 | 0.02 | 2 | 4.5 | 1.6 | 2 | 6.6 | 0.2 | 2 | 6.8 | 0.4 | 3 |
| Heart | 4.0 | | 1 | 3.0 | | 1 | 2.7 | 0.8 | 2 | 3.3 | 0.4 | 3 |
| Lungs | 9.3 | | 1 | 7.7 | | 1 | 6.2 | 3.2 | 2 | 5.8 | 1.4 | 3 |
| Liver | 5.3 | | 1 | 4.6 | | 1 | 4.7 | 0.3 | 2 | 6.4 | 0.7 | 3 |
| Spleen | 12.1 | | 1 | 11.4 | | 1 | 8.1 | 2.2 | 2 | 11.8 | 1.6 | 3 |
| Pancreas | 1.4 | | 1 | 1.3 | | 1 | 1.1 | 0.5 | 2 | 1.1 | 0.1 | 3 |
| Stomach | 1.5 | | 1 | 1.1 | | 1 | 1.0 | 0.03 | 2 | 0.8 | 0.2 | 3 |
| Small Intestine | 1.6 | | 1 | 1.5 | | 1 | 1.1 | 0.3 | 2 | 1.3 | 0.1 | 3 |
| Large Intestine | 1.1 | | 1 | 1.0 | | 1 | 0.8 | 0.1 | 2 | 0.9 | 0.1 | 3 |
| Kidney | 4.6 | | 1 | 4.6 | | 1 | 3.7 | 1.7 | 2 | 4.0 | 0.5 | 3 |
| Muscle | 1.2 | | 1 | 1.2 | | 1 | 0.8 | 0.3 | 2 | 0.7 | 0.1 | 3 |
| Bone | 5.6 | | 1 | 4.0 | | 1 | 4.7 | 2.6 | 2 | 3.9 | 0.5 | 3 |
| Skin | 5.4 | | 1 | 4.8 | | 1 | 3.4 | 1.1 | 2 | 5.8 | 1.4 | 3 |



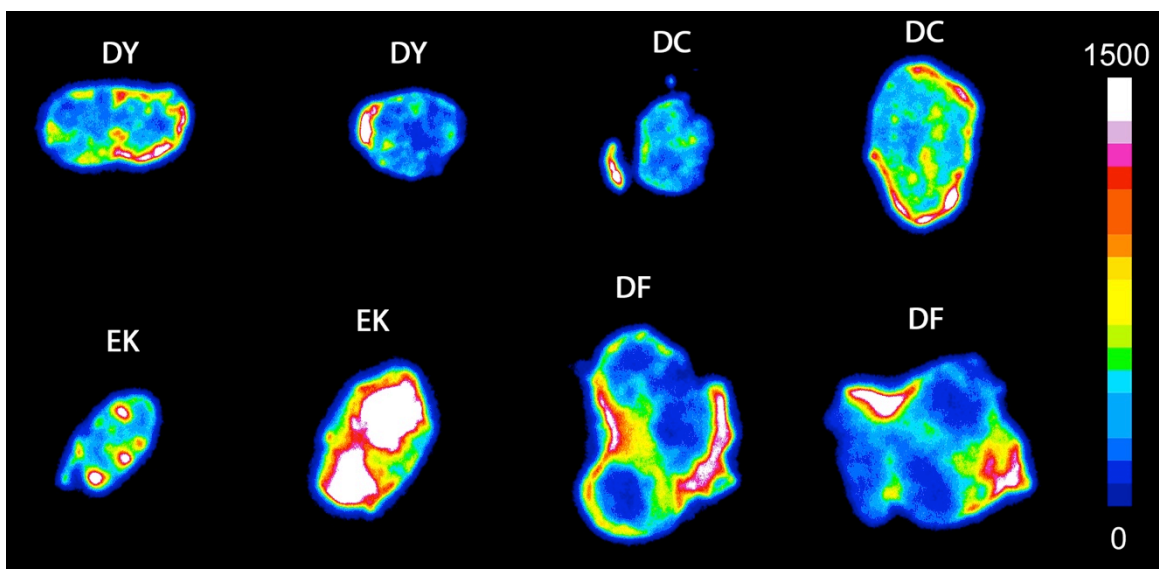
Supplemental Fig. 7. (A) a comparison of blocking and non-blocking groups from the biodistribution data of ⁸⁹Zr-DFO-AMG102 at 120 with data expressed as %ID, showing similar %ID values for all tissues except for statistically significantly less uptake in blocked tumors; and (B) a photograph of tumors from these biodistribution experiments showing the difference in size between groups. Data in Supplemental Tables 2-5, statistical significance shown from students unpaired t-test using PRISM software, * = ≤ 0.05 ** = ≤ 0.01 *** = ≤ 0.001.



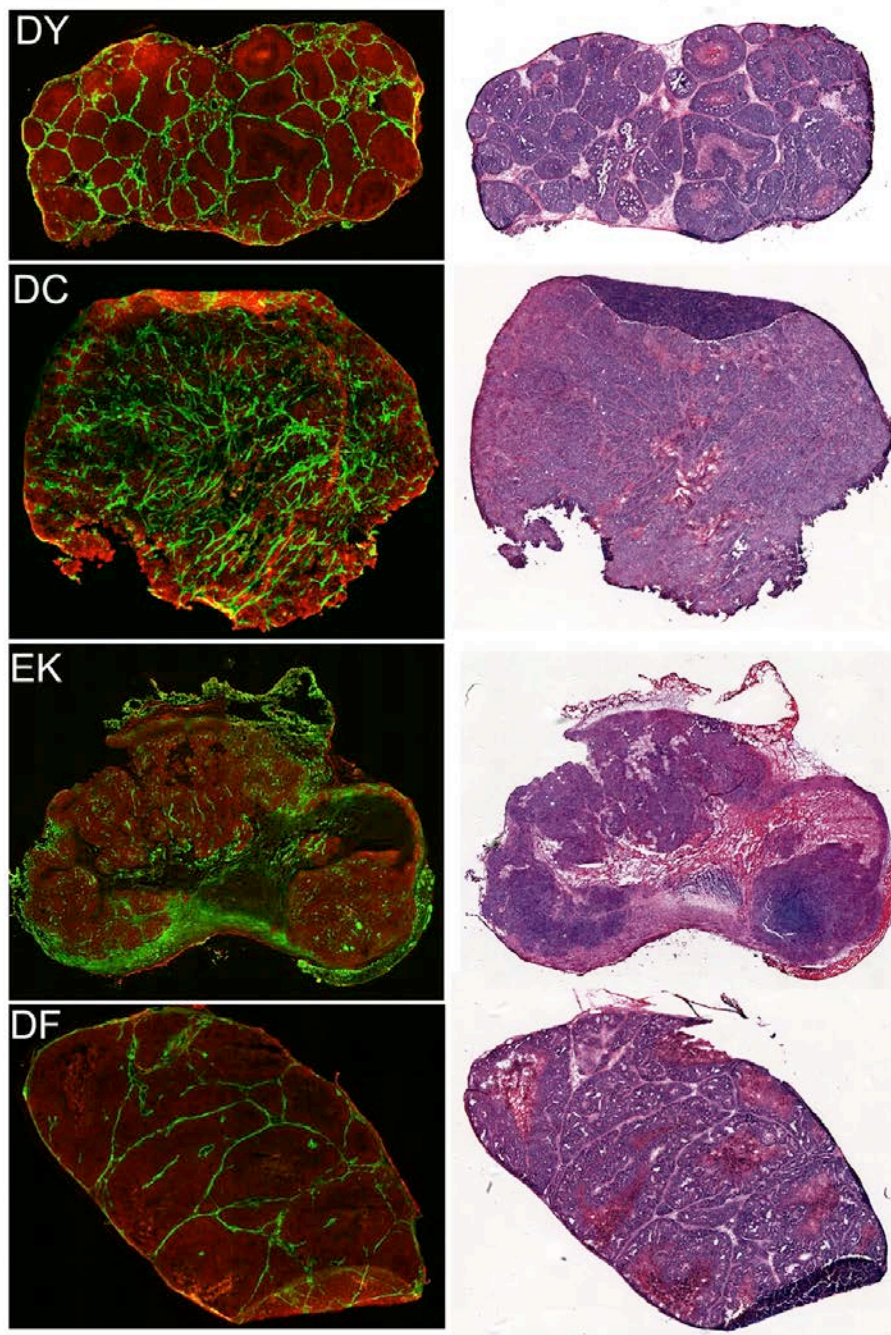
Supplemental Fig. 8. Serial PET imaging of ^{89}Zr -DFO-AMG102 in PDX DF and EK bearing mice with unknown levels of HGF at 24, 48, 72, and 120 h p.i. ($\sim 30 \mu\text{g}$, ~ 130 - $150 \mu\text{Ci}$, ~ 4.8 - 5.6 MBq , $200 \mu\text{L}$ sterile saline), showing low uptake in tumors suggesting very low levels of HGF protein, ~ 5 - 10 \%ID/g , EPR uptake only.



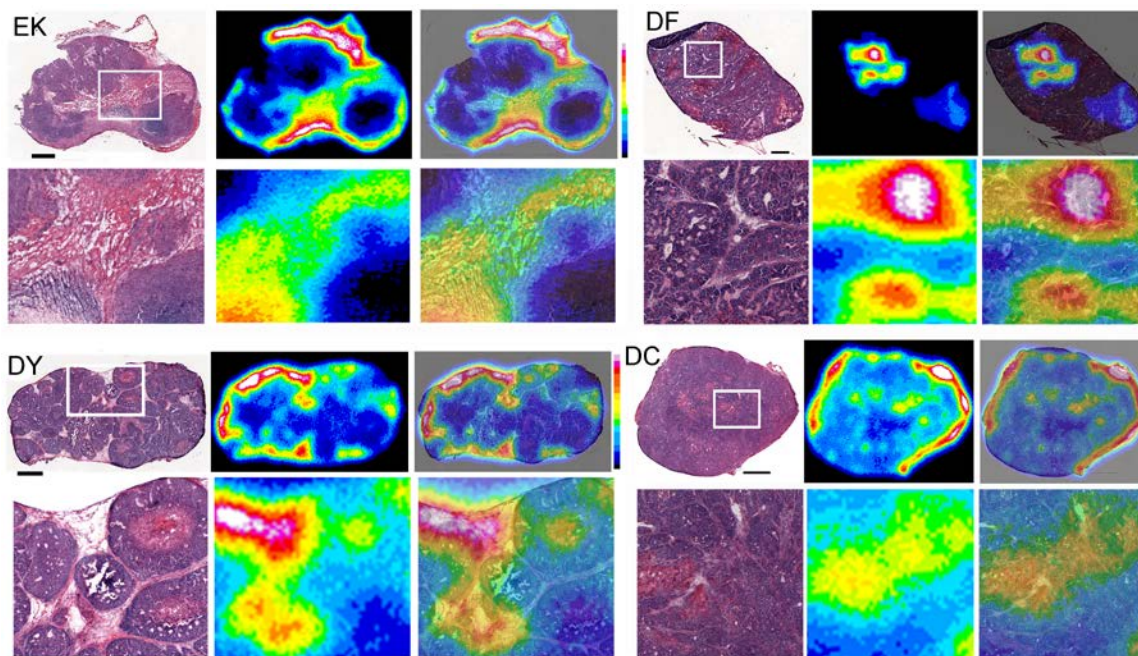
Supplemental Fig. 9. Serial PET imaging of ^{89}Zr -DFO-AMG102 in PDX DF and EK bearing mice with unknown levels of HGF at 24, 48, 72, and 120 h p.i. ($\sim 30\ \mu\text{g}$, $\sim 130\text{--}150\ \mu\text{Ci}$, $\sim 4.8\text{--}5.6\ \text{MBq}$, $200\ \mu\text{L}$ sterile saline), showing low uptake in tumors suggesting very low levels of HGF protein, $\sim 5\text{--}10\ \text{\%ID/g}$, EPR uptake only.



Supplemental Fig. 10. Autoradiography of ^{89}Zr -DFO-AMG102 in patient-derived xenograft mouse models (subcutaneous), obtained at time of necropsy (120 h p.i.) after PET imaging, with all tumor sections run on the same phosphor-plate to obtain relative radiation intensity.



Supplemental Fig. 11. Autoradiography of ^{89}Zr -DFO-AMG102 in patient-derived xenograft mouse models (subcutaneous), obtained at time of necropsy (120 h p.i.) after PET imaging, with the images displayed showing histology from hematoxylin and eosin staining (right), and immunofluorescence staining shown in green for perlecan (extracellular matrix/stroma) and red for anti-HGF antibody on the left, with all 4 tumors having very little HGF present (red color intensity not normalized for image acquisition time, meaning the gain has been artificially turned up to visualize the red color, and despite the intense red color there is very little HGF actually present, as confirmed by ELISA assay). HGF levels in these samples are similar to those observed in MKN45 shown in the manuscript Fig. 7.



Supplemental Fig. 12. Autoradiography of ^{89}Zr -DFO-AMG102 in patient-derived xenograft mouse models (subcutaneous), obtained at time of necropsy (120 h p.i.) after PET imaging, with the images displayed showing histology from hematoxylin and eosin staining (left), autoradiography (middle), and an overlap of both (right).

REFERENCES

1. Carlin, S.; Zhang, H.; Reese, M.; Ramos, N. N.; Chen, Q.; Ricketts, S.-A., A Comparison of the Imaging Characteristics and Microregional Distribution of 4 Hypoxia PET Tracers. *J. Nucl. Med.* **2014**, *55* (3), 515-521.